

1

2

3

4

5

6

7 Spatial variations in the stoichiometry and geochemistry of Miocene dolomite from

8 Grand Cayman: implications for the origin of island dolostone

9

10

11

12

Min Ren, Brian Jones

13

*Department of Earth and Atmospheric Sciences, University of Alberta, Edmonton,*

14

*Alberta, Canada T6G 2E3*

15

16

17

18

19

20

21 *E-mail address: mren@ualberta.ca*

22

23

**24 Abstract**

25           The Cayman Formation (Miocene), ~140 m thick on Grand Cayman, is  
26 incompletely dolomitized with the most of the dolomite restricted to the peripheral part of  
27 the island. These calcium-rich dolomites, with 50–60 mol %CaCO<sub>3</sub> (%Ca), are divided  
28 into low-calcium dolomite (LCD, %Ca < 55%) and high-calcium dolomite (HCD, %Ca  
29 >55%). Despite the small size of the island (6.8 km wide), the percentages of LCD and  
30 HCD, the %Ca, and the geochemical properties of the dolomites show geographic  
31 variations relative to the surrounding shelf edge. Accordingly, the Cayman Formation on  
32 the east end of the island is divided into the peripheral dolostone (shelf edge–1.5 km  
33 inland), transitional dolostone (1.5–2.7 km inland), and the interior limestone and  
34 dolostone (2.7 km to island center). From the peripheral dolostone to the interior  
35 limestone and dolostone, there is an increase in the percentage of HCD and %Ca in the  
36 dolomite, and decreases in the  $\delta^{18}\text{O}$  and  $\delta^{13}\text{C}$  values of the dolomite. Interpretations  
37 based on the oxygen and carbon isotopic compositions indicate that seawater is the  
38 source of Mg for dolomitization. The concentric pattern of dolomitization on the island  
39 reflects the fact that seawater flowed into the island from all directions during  
40 dolomitization. The lateral inland variations in the dolomite stoichiometric and isotopic  
41 properties reflect the gradual modification of seawater by water-rock interaction along  
42 the flow path from the shelf edge to the island center.  $^{87}\text{Sr}/^{86}\text{Sr}$  ratios indicate that two  
43 phases of dolomitization (late Miocene–early Pliocene and late Pliocene–early  
44 Pleistocene) were responsible for dolomitization of the Cayman Formation. It is very  
45 likely that during both phases, the carbonate platform was subaerially exposed and that  
46 the pump for circulating the seawater through the island was related to the

47 seawater/freshwater mixing zone. The dolomitization model developed from Grand  
48 Cayman may be applicable to many other island dolostones affected by long term sea-  
49 level changes. Given that the diagenetic potential of dolostone is directly linked to its  
50 stoichiometry, the distribution of the LCD-HCD will influence the petrographic  
51 properties, geochemical signatures, and reservoir potential of the dolostones.

52

53 **Keywords:** Dolomite; Dolomitization; Miocene; Stoichiometry; Grand Cayman

## 54 1. Introduction

55 Dolomite (ideally  $\text{CaMg}(\text{CO}_3)_2$ ), has received considerable attention because of questions  
56 that remain about its origin (Land and Moore, 1980; Budd, 1997; Warren, 2000; Machel, 2004;  
57 Gregg et al., 2015). Sedimentary dolomites typically contain excess calcium (48-62  
58 mol % $\text{CaCO}_3$ , hereafter referred to as %Ca), as is the case for most modern and Cenozoic  
59 dolostones (e.g., Vahrenkamp et al., 1994; Budd, 1997; Wheeler et al., 1999; Jones and Luth,  
60 2002; Suzuki et al., 2006). Many Phanerozoic dolomites, despite their antiquity, are still non-  
61 stoichiometric (e.g., Lumsden and Chimahusky, 1980; Sperber et al., 1984; Reeder, 1991; Drits  
62 et al., 2005; Swart et al., 2005). Calcium-rich dolomites are thermodynamically metastable and  
63 more reactive than ideal or near-stoichiometric dolomites (e.g., Reeder, 1991; Chai et al., 1995).  
64 Thus, in most geological environments HCD is more susceptible to diagenetic modifications than  
65 LCD (Jones and Luth, 2002). This includes the preferential dissolution of the calcium-rich cores  
66 found in many dolomite crystals. Dolostones formed of hollow crystals generated by this  
67 process have high micro-porosity (Jones and Luth, 2002; Jones, 2007) and may be important  
68 reservoir rocks. Later precipitation of calcite or dolomite in the hollow crystals leads to the  
69 formation of dedolomite (Schmidt, 1965; Folkman, 1969; Jones, 1989; James et al., 1993) or  
70 inside-out dolomite (Jones, 2007). At burial, non-stoichiometric dolomite is prone to  
71 recrystallization and transformation to stoichiometric, well-ordered dolomites (e.g., Land and  
72 Moore, 1980; Reeder, 1981; Blake et al., 1982; Hardie, 1987; Kaczmarek and Sibley, 2014).  
73 Such modifications change the petrographic properties, geochemical signatures, and reservoir  
74 potential of the dolostones.

75 Models developed to explain dolomitization have typically regarded dolostones as being  
76 compositionally uniform. In many cases, however, two or more dolomite populations, as defined

77 by their composition, are present (Sperber et al., 1984; Searl, 1994; Wheeler et al., 1999; Jones  
78 and Luth, 2002; Drits et al., 2005; Suzuki et al., 2006). If variations in stoichiometry have been  
79 considered, it is done from a stratigraphic perspective and the possibility of geographic variations  
80 have been ignored (e.g., Dawans and Swart, 1988; Wheeler et al., 1999). Cenozoic dolostones  
81 on the Cayman Islands, which are formed of various mixtures of low calcium dolomite  
82 (LCD, %Ca = 48-55%) and high calcium dolomite (HCD, %Ca = 55-62%) (Jones et al., 2001;  
83 Jones, 2005, 2013), are ideal for testing the notion that lateral variations in the composition of  
84 dolostones may be critical for developing a model to explain their origin. On east end of Grand  
85 Cayman, 32 wells drilled and sampled to depths up to 140 m, are ideally suited for establishing  
86 the stratigraphic and geographic variations in the %Ca of dolostones on an isolated carbonate  
87 island. The model developed to explain the formation of these island dolostones is based on the  
88 integration of their petrography, %Ca, stable isotopes,  $^{87}\text{Sr}/^{86}\text{Sr}$  isotopes, and stratigraphic  
89 relationships with coeval limestones. The model, which also relies on the chemistry of the  
90 present-day groundwater, is also used to test some of the basic concepts of dolomite formation  
91 that have been derived from laboratory experiments like those described by Kaszmarek and  
92 Sibley (2011, 2014). The conclusions reached by this research have far reaching implications for  
93 the development of island dolostones throughout the world.

## 94 **2. Geological setting**

95 Grand Cayman, located on the Cayman Ridge in the Caribbean Sea (Fig. 1A), is  
96 surrounded by a shelf that is < 1 km wide (Fig. 1B, C). Sculptured by two submarine terraces at  
97 0-10 m bsl and 12-40 m below sea level (bsl) (Fig. 1D), the shelf formed as a result of reef  
98 growth and marine erosion during successive sea-level cycles of the last deglaciation (e.g.,  
99 Blanchon and Jones, 1995). The island slope, which generally begins at a depth of ~55 m

100 (Roberts, 1994), extends into the deep Cayman Trench to the south and Yucatan Basin to the  
101 north. Today, the east end of the island has a N-S width of ~ 6.8 km. The low-lying interior of  
102 eastern part of this island, generally < 3 m above sea level (asl), is surrounded by a peripheral  
103 rim that is up to 13.5 m asl (e.g., Jones et al., 1994a; Jones and Hunter, 1994; Liang and Jones,  
104 2014).

105 The carbonate succession on Grand Cayman is divided into the unconformity-bounded  
106 Brac Formation, Cayman Formation, Pedro Castle Formation, and Ironshore Formation (Fig. 2).  
107 Limestones and dolostones of the Cayman Formation (Miocene) are widely exposed over the  
108 eastern part of the island (Fig. 1B). Fossils in this formation include corals, bivalves, red algae,  
109 foraminifera, and *Halimeda* (Jones et al., 1994b; Ren and Jones, 2016) (Fig. 2). On the east end,  
110 the Cayman formation has undergone pervasive dolomitization in the coastal areas but minimal  
111 dolomitization in the central areas of the island (Der, 2012; Ren and Jones, 2016).

### 112 3. Methods

113 This paper integrates all information from outcrops and 32 wells on the east end of Grand  
114 Cayman with focus being placed on 21 wells (Fig. 1C, E; Table 1), which were selected because  
115 they are the deepest wells (40 to 140 m with most > 70 m) and are located at various distances  
116 from the shoreline. Continuous cores were obtained from wells GFN-2 and RWP-2. Cuttings  
117 were collected over 0.8 m (2.5 ft) intervals from all other wells. The depth of each well is  
118 accurate to  $\pm 1\%$  whereas the depth intervals represented by each sample of cuttings are  $\pm 2\%$   
119 with the highest variance being on the deeper samples.

120 Petrographic descriptions are based on standard thin-section techniques and scanning  
121 electron microscopy. Thin sections, made from 120 samples from GFN-2, RWP-2, HRQ-3, and  
122 RTR-1, were impregnated with blue epoxy to highlight porosity and stained with Alizarin Red S

123 to indicate calcite. Thicker (40-50  $\mu\text{m}$ ) thin sections from selected samples from HRQ-2 were  
124 prepared for examination on the SEM. After these epoxy-impregnated thin sections were  
125 polished and etched in 30% HCl for 10-15 seconds following the procedure outlined by Jones  
126 (2005), they were then coated with carbon and examined on a Zeiss EVO SEM (LaB<sub>6</sub> electron  
127 source, accelerating voltage 15 kV). Backscattered electron (BSE) images were obtained from  
128 these samples. Elemental compositions were obtained from spots/lines/areas using a Bruker  
129 energy dispersive X-ray spectroscopy (EDS) system with dual silicon drift detectors, each with  
130 an area of 60 mm<sup>2</sup> and an energy resolution of 123 eV.

131 Rock cuttings (collected over 1.5 m intervals), formed largely of matrix dolostone or  
132 limestone (fossils and/or cement were avoided), were ground into a fine powder using a mortar  
133 and pestle and then subjected to X-ray diffraction (XRD) using a Rigaku Geigerflex 2173 XRD  
134 system with Co K $\alpha$  radiation from 29° to 38° 2 $\theta$  at 40 kV and 35 mA following the protocol of  
135 Jones et al. (2001). The peak-fitting method of Jones et al. (2001) was used to determine the  
136 %Ca of the constituent LCD and HCD ( $\pm 0.5\%$  accuracy) and the weight percentages of LCD and  
137 HCD ( $\pm 10\%$  accuracy).

138 Oxygen and carbon isotopes for the dolomite and calcite were determined for every other  
139 XRD sample (i.e., at 3 m intervals) from EEZ-1, CKC-1, LBL-1, HMB-1, HRQ-1, HRQ-2, and  
140 HRQ-3. These analyses were undertaken by Isotope Tracer Technologies Inc. (Waterloo,  
141 Canada) who used a DELTA<sup>Plus</sup> XL Stable Isotope Ratio Mass Spectrometer (IRMS) coupled  
142 with a ConFlo III interface and EA1110 Elemental Analyzer. No phosphoric acid fractionation  
143 factor was applied to the dolomite. The isotopes are reported relative to VPDB in per mill  
144 ( $\pm 0.1\text{‰}$  accuracy).

145  $^{87}\text{Sr}/^{86}\text{Sr}$  were measured for 114 samples from RWP-2, FFM-1, HMB-1, CKC-1, RTR-1,  
146 and GFN-2 in the Radiogenetic Isotope Laboratory, University of Alberta, using the same  
147 procedure as MacNeil and Jones (2003). All results were corrected for variable mass  
148 discrimination (0.1194) and normalized to SRM 987 standard (0.710245). The 2 standard errors  
149 of the  $^{87}\text{Sr}/^{86}\text{Sr}$  values range from 0.00001 to 0.00003.

150 Groundwater samples were collected from RTR-1 (2009), GFN-1 (2011), and HRQ-3  
151 (2014); and seawater samples from Spotts Bay (south coast) were also collected in each of these  
152 years. Chemical composition and oxygen isotope analyses were performed for 34 groundwater  
153 and 3 seawater samples by the Saskatchewan Research Council and Isotope Tracer Technologies  
154 Inc., respectively, within 2 months of collection. Saline water is defined using chloride contents  
155 (>19,000 mg/L) following Ng et al. (1992). Ninety-seven groundwater samples were measured  
156 for temperature during drilling of GFN-1, HRQ-2, and EEV-2.

## 157 **4. Results**

### 158 *4.1. Sedimentary facies*

159 The Cayman Formation contains numerous fossils including corals (mainly *Stylophora*,  
160 *Montastrea*, *Porites*), benthic foraminifera, bivalves, gastropods, red algae, and planktonic  
161 foraminifera. Der (2012) and Ren and Jones (2016) recognized the following biofacies: (1)  
162 rhodolith-coral-benthic foraminifera, (2) platy and domal coral–benthic foraminifera, (3)  
163 branching platy and domal coral–benthic foraminifera, (4) branching coral-benthic foraminifera  
164 facies, (5) benthic foraminifera-bivalve, (6) *Halimeda*-benthic foraminifera–coral, and (7)  
165 planktonic foraminifera facies (Fig. 3). Facies 1 is found only in two coastal wells (RWP-2 and  
166 RTR-1), facies 2, 3, and 4 are found in most wells but are most common in the coastal areas, and

167 facies 6 and 7 are present only in GFN-2 and HRQ-2, which are located in the interior of the  
168 island (Fig. 3).

#### 169 *4.2. Definition and distribution of the dolostone and limestone*

170 The Cayman Formation contains undolomitized limestones, partially dolomitized  
171 limestones, and dolostones. Most dolostone is found around the perimeter of the island and in  
172 the shallow surface zone in the interior of the island, whereas limestones are restricted to the  
173 interior part of the island (Figs. 4, 5). There is no evidence indicating that the limestone and  
174 dolostones belong to different formations (Ren and Jones, 2016).

175 Key attributes of each succession are the distribution of LCD, HCD, and calcite. Well  
176 locations are specified relative to shelf edge rather than the present-day coastline, which is a  
177 feature of recent erosion and sea level. Integration of the geographic positions of the wells and  
178 their basic lithological attributes allows delineation of the (1) peripheral dolostone zone, (2)  
179 transitional dolostone zone, (3) interior dolostone zone, and (4) interior limestone zone (Fig. 6).

180 The “peripheral zone” includes areas that are within ~1.5 km from the present-day N and  
181 S shelf edges and ~2 km from the E shelf margin (Fig. 6). Wells HHD-1, LBL-1, RWP-2, EEZ-  
182 1, ESS-1, HMB-1, and RTR-1 are located in the zone. Given its position and that the subsurface  
183 Cayman Formation in these locations is comprised of dolostone, this zone is referred to as the  
184 peripheral dolostone zone (Fig. 6). These successions are dominated by LCD, with many being  
185 formed entirely of LCD-dominated dolostones (e.g., LBL-1, RWP-2, EEZ-1, FSR-1).

186 The “transitional zone”, located between the inner boundary of peripheral zone to ~2.7  
187 km from the N and S shelf edges, and ~3 km from the E shelf edge, includes wells CKC-1, EEV-  
188 2, HRQ-3, and FSR-1 (Fig. 6). It is named the transitional dolostone zone because the Cayman  
189 Formation in the area is formed of LCD- and HCD-dominated dolostones (Fig. 6).

190 The “interior zone”, found in the innermost part of the island, is interior of the  
191 transitional zone and includes wells FFM-1, GFN-2, HRQ-2, HRQ-1, HRQ-4, HRQ-5, HRQ-6,  
192 HRQ-7, HRQ-8, and DTE-1 (Fig. 6). The Cayman Formation in this zone is comprised of  
193 limestones and calcian dolostones. The limestones, which are found in all of the wells in this  
194 area, are referred to as the interior limestones. In some wells, limestone forms the entire  
195 succession, whereas in other wells it is restricted to the deeper part of successions (Fig. 6). The  
196 boundary between these dolostones and limestones lies somewhere between wells CLZ-1 and  
197 HMB-1. Dolostones that lie on top of the limestone successions in the eastern interior (e.g.,  
198 HRQ-2, FFM-1, GFN-2), formed largely of HCD, are referred to as the interior dolostones.

#### 199 *4.3. Distribution of calcite cements*

200 The distribution of calcitic sediments and calcite cements in the Cayman Formation in the  
201 central part of the island is variable. This upper dolostone unit (~15 m thick), found on the  
202 eastern part of the island as in wells GFN-2, RWP-2 (Ren and Jones, 2016) and HRQ-3 (Fig. 7A-  
203 C), is characterized by calcite cement that fills cavities and pores. The calcite cement, dominated  
204 by blocky crystals (50-100  $\mu\text{m}$  long), postdated pervasive dolomitization (Ren and Jones, 2016).  
205 The volume of calcite cement depends on the porosity and permeability of the host rock. In well  
206 GFN-2, for example, the calcite cement forms up to 40% of the porous calcareous dolostones. In  
207 contrast, the less permeable peripheral dolostones, like those in RWP-2, contain < 3% calcite  
208 cement.

209 In the interior wells, like GFN-2 and HRQ-2, the lower part of the Cayman Formation is  
210 formed of original limestones with only minor amounts of calcite cement (Fig. 7D-F). The depth  
211 to the upper boundary of this unit varies from ~55 m bsl in the HRQ wells to ~8 m bsl in GFN-2.  
212 In this unit, most of the aragonite skeletons were dissolved and resultant porosity is high (e.g.,

213 50% in well GFN-2). Although the lower boundary of this unit is unknown, it continues to the  
214 base of well HRQ-2 at 125 m bsl.

#### 215 4.4. Dolomite petrography

216 Dolostones in the Cayman Formation are petrographically heterogeneous and range from  
217 fabric retentive to fabric destructive (Figs. 8-10). Based on the preservation of precursor fabrics  
218 and the amount of dolomite cement, three textures are recognized.

- 219 • Fabric retentive and pervasively cemented dolostones (Fig. 8), common in the peripheral  
220 dolostone zone, are typically light gray-brown and well indurated. Corals, red algae, and  
221 foraminifera are well preserved and replaced by subhedral-anhedral dolomite crystals that  
222 are < 10  $\mu\text{m}$  long. Limpid dolomite cements, forming up to 50% of the rock (commonly  
223 20-25%), are characterized by tightly interlocking subhedral to euhedral crystals that are up  
224 to 100  $\mu\text{m}$  long but typically 25-30  $\mu\text{m}$  long (Fig. 8B, C). Individual crystals commonly  
225 have alternating LCD-HCD zones (each  $\sim$  5  $\mu\text{m}$  thick). Porosity, typically <10%, includes  
226 mainly inter- and intra-particle types and fossil moldic porosity is rare.
- 227 • Fabric retentive to destructive and poorly cemented dolostones (Fig. 9A-D), common in the  
228 transitional and interior dolostones, are white and poorly indurated. The precursor  
229 carbonate fabrics are typically moderately to well preserved, being replaced by dolomite  
230 crystals that are < 10  $\mu\text{m}$  long (Fig. 9A). Locally, however, some fabrics are poorly  
231 preserved (Fig. 9B, C). Widespread dissolution of the aragonitic components means that  
232 fossil-moldic porosity is common (Fig. 9B). Limpid dolomite is rare with only scattered  
233 euhedral-subhedral crystals (20-25  $\mu\text{m}$  long) lining some cavities. Porosity is high (up to  
234  $\sim$ 40%) and dominated by primary and fossil moldic porosity.

- 235 • Dolomite in the interior limestone, which partly replaced some skeletal grains, consists of  
236 euohedral to subohedral crystals that are < 15  $\mu\text{m}$  long (Fig. 9E, F). Dissolution, which is  
237 common, left scattered clusters of dolomite crystals in the chambers of some biofragments.  
238 There is no dolomite cement. Fossil moldic porosity dominates.

#### 239 4.5. Dolomite stoichiometry

240 Dolostones in the Cayman Formation are composed of pure LCD (%LCD =100), pure  
241 HCD (%HCD=100), or mixed LCD and HCD. The distribution of LCD, HCD, and mixed LCD-  
242 HCD is variable at all scales, ranging from individual crystals (microns) to island scale  
243 (kilometres).

##### 244 4.5.1. LCD-HCD – crystal scale

245 Dolomites in the peripheral dolostones are characterized by a variety of LCD-HCD  
246 patterns similar to those found in the Cayman Formation on the west part of Grand Cayman (cf.,  
247 Jones and Luth, 2002). Dolomite crystals, up to 100  $\mu\text{m}$  (typically 50  $\mu\text{m}$  long), commonly have  
248 cores formed of HCD and cortices formed of LCD or alternating LCD and HCD zones. Pore-  
249 lining and pore-filling limpid dolomite crystals are formed of LCD or alternating LCD and HCD  
250 zones.

251 In the interior dolostone, most dolomite crystals (< 20  $\mu\text{m}$  long with most 5-10  $\mu\text{m}$  long)  
252 are formed entirely of HCD (Fig. 11). Euohedral to subohedral LCD pore-filling crystals (< 15  $\mu\text{m}$   
253 long) are locally present. Rare dolomite crystals have HCD cores encrusted by LCD cortices that  
254 are < 3  $\mu\text{m}$  thick. The dolomite crystals are characterized by a variety of surface microstructures  
255 such as dissolution slots and etch pits (Fig. 11), like those documented by Jones (2013).

256 4.5.2. *LCD-HCD – local scale*

257 High Rock Quarry, located in the center of the eastern part of Grand Cayman, is ~1.3 km  
258 long E-W and ~1 km wide N-S (Fig. 1C, E). Analyses of samples from 8 closely spaced wells in  
259 this quarry show some stratigraphic and spatial patterns to the distribution of the LCD and HCD  
260 over distances of < 600 m (Fig. 12). In HRQ-5, for example, the dolostones that form the upper  
261 70 m of the succession (Fig. 12) include (1) HCD dolostone from 41.5 to 70 m, (2) LCD  
262 dolostone from 26.3 to 41.5 m, (3) HCD dolostone from 17.1 to 26.3 m, and (4) LCD dolostone  
263 from 0 to 17.1 m.

264 Although the stacking patterns of the dolomite units, as defined by their LCD–HCD  
265 ratios, varies from well to well, some closely spaced wells such as HRQ-1, HRQ-2, HRQ-4, and  
266 HRQ-5, display similar mineralogical patterns (Fig. 12). This pattern, as illustrated in HRQ-5, is  
267 characterized by four alternating LCD-HCD units that start with a HCD unit at the bottom of the  
268 well and ends with a LCD unit near surface (Fig. 12). HRQ-4 and HRQ-5, which are only 140 m  
269 apart, are almost identical in terms of thicknesses, %Ca in LCD and HCD, and average %Ca  
270 (Fig. 12). In the calcian dolostones or dolomitic limestones, calcite is commonly found with the  
271 HCD but is rarely associated with the LCD.

272 4.5.3. *LCD-HCD – island-wide scale*

273 Most dolostones in the Cayman Formation are formed of LCD and HCD, typically with  
274 one type being dominant (Figs. 13-15). Samples formed of subequal amounts of LCD and HCD  
275 are rare. The compositions of the dolostones varies geographically between the peripheral,  
276 transitional, and central zones (Figs. 13-15).

277 (1) Peripheral dolostones in HHD-1, LBL-1, RWP-2, EEZ-1, ESS-1, and HMB-1 are  
278 dominated by LCD except for RTR-1, where LCD-dominated dolostones forms only 50%

279 of the succession (Figs. 13, 17A). LCD-dominated dolostones form all of the successions in  
280 LBL-1, RWP-2, and EEZ-1, 95% in ESS-1, 94% in HHD-1, 87% in HMB-1. Of the 421  
281 peripheral dolostone samples in these 7 wells, 79% are LCD-dominated with most  
282 containing 80–90 %LCD (Fig. 17A).

283 (2) Transitional dolostones in the CKC-1, HRQ-3, EEV-2, and FSR-1 generally contain LCD  
284 and HCD with the composition of the dolostones varying from well to well (Figs. 14, 17B).  
285 In the dolostone successions from CKC-1 and HRQ-3, the LCD-dominated dolostone  
286 forms 88% and 90% of the succession, respectively (Fig. 14). In EEV-2 and FSR-1, which  
287 are closer to the southern coastline, the dolostone successions are formed entirely of HCD-  
288 dominated dolostones (Fig. 14). Of the 190 samples from these wells, 74% of the  
289 dolostones are LCD-dominated with most composed of 80-90%LCD (Fig. 17B).

290 (3) Interior dolostones, including those from FFM-1, GFN-2, HRQ-1, HRQ-2, HRQ-4, HRQ-5,  
291 HRQ-6, HRQ-7, and HRQ-8, differ from the peripheral and transitional dolostones because  
292 apart from HRG-7, they all contain more HCD than LCD (Figs. 15, 17C). The average  
293 %HCD in dolostones from FFM-1 is 98.4%, whereas in the remaining wells it is 54.7-  
294 63.9% (Fig. 15). The average %HCD (42.0%) in the dolostones from HRQ-7 is misleading  
295 because that well is only 39.6 m deep and does not cover the full depth range of the other  
296 wells (Fig. 12). The average %HCD from 341 dolostone samples in these 9 wells is 42-  
297 98% (Fig. 15) and 65% of the 341 analyzed dolomite samples contain more HCD than  
298 LCD (Fig. 17C). Forty-five samples are formed of HCD alone.

299 (4) Interior limestones that contain some dolomite are dominated by HCD (Figs. 16, 17D). Of  
300 the 191 analyzed samples, dolomite was found in 186 of them with HCD dominating in  
301 93% of them (Fig. 17D). LCD was found only in well HRQ-2 (Fig. 16).

302 At the island-wide scale, there is no readily apparent stratigraphic pattern to the  
303 distribution of the LCD and HCD (Figs. 4, 5). It seems, however, that the dolostones that overlie  
304 and/or underlie limestone successions are invariably dominated by HCD (Figs. 4, 5).

#### 305 4.6. Oxygen and carbon isotopes

306 Dolomite from 206 samples in eight wells have  $\delta^{18}\text{O}$  from 0.68‰ to 5.03‰ (average =  
307  $3.12 \pm 1.02\text{‰}$ ) and  $\delta^{13}\text{C}$  ranging from 0.52 to 3.83‰ (average =  $2.37 \pm 0.84\text{‰}$ ) (Fig. 18A). For  
308 dolomites in the calcian dolostones, the  $\delta^{18}\text{O}$  ranges from 1.11‰ to 5.03‰ (average =  $3.26 \pm$   
309  $0.94\text{‰}$ , n=182), and the  $\delta^{13}\text{C}$  ranges from 0.52 to 3.83‰ (average =  $2.50 \pm 0.80\text{‰}$ , n=182). In  
310 contrast, the  $\delta^{18}\text{O}$  values for dolomite in the dolomitic limestones range from 0.68‰ to 3.84‰  
311 (average =  $2.10 \pm 1.03\text{‰}$ , n=24), and the  $\delta^{13}\text{C}$  ranges from 0.64 to 2.15‰ (average =  $1.42 \pm$   
312  $0.43\text{‰}$ , n=24).

313 The dolomites in the three geographically defined dolostone zones and the limestone are  
314 characterized by isotopic compositions that become progressively more positive towards the  
315 interior of the island (Fig. 18B).

316 (1) Peripheral dolostone – 105 dolomites from RWP-2, HMB-1, EEZ-1, and LBL-1 have high  
317  $\delta^{18}\text{O}$  (1.11 to 5.03‰, mean =  $3.62 \pm 0.85\text{‰}$ ) and  $\delta^{13}\text{C}$  (1.32 to 3.83‰, mean =  $3.05 \pm$   
318  $0.47\text{‰}$ ) values.

319 (2) Transitional dolostone – 41 dolomites from HRQ-3 and CKC-1 are characterized by  
320 intermediate  $\delta^{18}\text{O}$  (1.29 to 4.73‰, mean =  $3.10 \pm 0.88\text{‰}$ ) and  $\delta^{13}\text{C}$  (0.94 to 3.29‰, mean =  
321  $2.01 \pm 0.44\text{‰}$ ) values.

322 (3) Interior dolostone – 36 dolomites from HRQ-1 (0 to 55 m) and HRQ-2 (0-54 m) have  $\delta^{18}\text{O}$   
323 values from 1.36 to 3.46‰ (mean =  $2.37 \pm 0.55\text{‰}$ ), and  $\delta^{13}\text{C}$  values from 0.52 to 2.33‰

324 (mean =  $1.46 \pm 0.40\%$ ). Although there is some overlap between the isotopes of interior  
325 and transitional dolostones, the former is generally lower than the latter, (Fig. 18C).

326 (4) Interior limestone – 24 dolomites in limestones from HRQ-1 (55-60 m) and HRQ-2 (54-  
327 127 m) have the lowest  $\delta^{18}\text{O}$  (0.68 to 3.84‰, mean =  $2.10 \pm 1.03\%$ ) and  $\delta^{13}\text{C}$  (0.64 to 2.15  
328 ‰, mean =  $1.42 \pm 0.43\%$ ) values.

329 The oxygen and carbon isotopes from the peripheral dolostones display no apparent co-  
330 variation between the  $\delta^{18}\text{O}$  and  $\delta^{13}\text{C}$  values (Fig. 18A). In contrast, there is a positive co-  
331 variation between the two isotopes for dolomite in the transitional dolostone in CKC-1 ( $r^2=0.67$ )  
332 and HRQ-3 ( $r^2=0.30$ ) and in the interior dolostone and limestone from HRQ-2 ( $r^2=0.50$ ) (Fig.  
333 19).

334 Overall, the  $\delta^{18}\text{O}$  and  $\delta^{13}\text{C}$  values of the dolomites are poorly correlated with the average  
335 %Ca (Fig. 20A, B). For those dolomites formed almost entirely of LCD (%LCD > 90%) or  
336 HCD (%HCD > 90%), there is no obvious correlation between their  $\delta^{18}\text{O}$  values and %Ca (Fig.  
337 20C). The average  $\delta^{18}\text{O}$  of 45 dolomite samples with LCD>90% (wells LBL-1, RWP-2, EEZ-1,  
338 CKC-1, HRQ-3, and HMB-1) is  $2.97 \pm 0.53\%$ ; whereas the average  $\delta^{18}\text{O}$  value for all 19  
339 dolomite samples with HCD>90% (wells CKC-1, HRQ-1, HRQ-2, HRQ-3, and HMB-1) is  
340 0.75‰ lower ( $2.22 \pm 0.33\%$ ; Fig. 20C).

341 In all of the wells, the  $\delta^{18}\text{O}$  and  $\delta^{13}\text{C}$  values of the dolomites increase with depth (Fig. 21).  
342 The rate of increase is commonly highest near the surface. In RWP-2, LBL-1, and HMB-1, for  
343 example, the increase in  $\delta^{18}\text{O}$  from 10 to 20 m can be 1.0 to 1.5‰. Although apparent in each  
344 well, the rate of  $\delta^{18}\text{O}$  increase with depth varies from well to well. For example, in the deeper  
345 part of the successions, the increases in  $\delta^{18}\text{O}$  are higher in CKC-1, HMB-1, and HRQ-2 (increase  
346 ~ 1‰ in 30 m) than in the other wells (Fig. 21).

347           There is a good correlation between the  $\delta^{18}\text{O}$  values of the dolomite and the associated  
348 calcite in well HRQ-2 (average  $\Delta^{18}\text{O}_{\text{dol-cal}} = 1.75\text{‰}$ ,  $n=24$ ; Fig. 22A). Similarly, the  $\delta^{13}\text{C}$  values  
349 of the dolomite are  $\sim 0.60\text{‰}$  higher than the coexisting calcite from the same well (Fig. 22B).

#### 350 *4.7. Strontium isotopes*

351           Collectively, the  $^{87}\text{Sr}/^{86}\text{Sr}$  ratios of the 100% dolomite samples, which range from  
352 0.70888 to 0.70914 (average = 0.70902,  $n = 104$ ), have a unimodal distribution with a mode of  
353 0.70900-0.70902 (Fig. 23A). Nevertheless, the  $^{87}\text{Sr}/^{86}\text{Sr}$  ratios vary from well to well. In the  
354 peripheral dolostones, an obvious bimodal distribution of the  $^{87}\text{Sr}/^{86}\text{Sr}$  is apparent in well HMB-1  
355 (modes at 0.70896-0.70898 and 0.70906-0.70908), whereas in RWP-2 and RTR-1 there is no  
356 bimodality (Fig. 23B-D). The transitional dolostones from CKC-1 have a bimodal distribution  
357 of  $^{87}\text{Sr}/^{86}\text{Sr}$  with the modes at 0.70900-0.70902 and 0.70908-0.70910 (Fig. 23E). In contrast, the  
358 interior dolostones from well FFM-1 have a unimodal distribution of  $^{87}\text{Sr}/^{86}\text{Sr}$  with the mode at  
359 0.70908-0.70910 (Fig. 23F).

360           There is no obvious correlation between the  $^{87}\text{Sr}/^{86}\text{Sr}$  values and the %LCD or the  
361 average %Ca of the dolostones (Fig. 24).

362           Two pure limestone samples from GFN-2 have  $^{87}\text{Sr}/^{86}\text{Sr}$  values of 0.70902 and 0.70915.  
363 The ratios from the 17 dolomitic limestones from FFM-1 and GFN-2 range from 0.70902 to  
364 0.70912 (average=0.70904) (Fig. 23A).

#### 365 *4.8. Groundwater geochemistry and temperature*

366           Today, the groundwater in the Cayman Formation on the east end of Grand Cayman  
367 includes the freshwater, saline, and brackish zones. A freshwater lens, centrally located on the  
368 east end of Grand Cayman (e.g., Mather, 1971; Ng et al., 1992) (Fig. 1B), is  $< 20$  m thick and

369 separated from the underlying saline zone by a mixing zone that is ~20 m thick (Ng and Jones,  
370 1995).

371 The water properties of the saline zone vary from location to location. Present-day  
372 seawater around Grand Cayman has an average Mg/Ca ratio of 5.4 (based on 3 samples collected  
373 from Spotts Bay) and contrasts with the ratios of groundwater from (1) RTR-1:  $4.95 \pm 0.20$  (n=5),  
374 (2) HRQ-3:  $4.38 \pm 0.34$  (n=7), and (3) GFN-1:  $3.60 \pm 0.13$  (n=10) (Fig. 25A). Compared with  
375 seawater collected around the island, the lower Mg/ca ratios of groundwater in these three wells  
376 are the result of a decrease in Mg and an increase in Ca (Fig. 25B).

377 The average  $\delta^{18}\text{O}_{\text{SMOW}}$  of the saline water from RTR-1, HRQ-3, and GFN-1 are  
378  $1.51 \pm 0.35\text{‰}$  (n=12),  $0.80 \pm 0.03\text{‰}$  (n=8), and  $0.67 \pm 0.08\text{‰}$  (n=5), respectively (Fig. 25C). There  
379 is no correlation between the  $\delta^{18}\text{O}$  of the water and the chloride concentration or the rock type in  
380 which it resides. The average  $\delta^{18}\text{O}$  of three seawater samples collected in Spotts Bay is 1.06‰.

381 Groundwater temperature changes with depth and location (Fig. 25D). The rate of  
382 decrease with depth is variable, being about  $-2^\circ\text{C}/10\text{m}$  within ~10 m bsl and about  $-2.5^\circ\text{C}/100$   
383 m from ~10 m bsl to the base of GFN-1 at ~120 m bsl. The water temperature in HRQ-3 and  
384 GFN-1, located in the island interior, is 1.5 to 2.0°C lower than that in EEV-2 at the same depth.

## 385 **5. Interpretation of dolomitizing time and fluids**

### 386 *5.1. Time of dolomitization*

387 Interpretation of the number of dolomitization phases and the exact timing of each phase  
388 is limited by the dating method employed. The error margin associated with  $^{87}\text{Sr}/^{86}\text{Sr}$  dating is  
389 typically  $> 0.5$  Ma and can be as high as 2 Ma if the data coincides with the plateaus on the  
390  $^{87}\text{Sr}/^{86}\text{Sr}$  curve (Jones and Luth, 2003b). The unimodal distribution of  $^{87}\text{Sr}/^{86}\text{Sr}$  (0.70900-0.7090)  
391 from all the dolostones in the Cayman Formation on the east end of Grand Cayman (Fig. 23A) is

392 similar to the unimodal histograms of Pleydell et al. (1990) and Jones and Luth (2003b) that had  
393 modes of 0.70900-0.70905 and 0.709025-0.709050, respectively. The large range in the  
394  $^{87}\text{Sr}/^{86}\text{Sr}$  values, however, means that two or even more phases of dolomitization may be  
395 included (Budd, 1997; Machel, 2000; Jones and Luth, 2003b).

396 For individual wells, the distribution of the  $^{87}\text{Sr}/^{86}\text{Sr}$  values for the dolostones varies. The  
397  $^{87}\text{Sr}/^{86}\text{Sr}$  values of peripheral dolostones in RWP-1 and RTR-1 range from 0.70888-0.70902 with  
398 a unimodal distribution (Fig. 23B, C), which may reflect the mixing of  $^{87}\text{Sr}/^{86}\text{Sr}$  values from  
399 more than one dolomitizing phases. Despite that, the peripheral dolostones in HMB-1 and the  
400 transitional dolostones in CKC-1 show bimodality of the  $^{87}\text{Sr}/^{86}\text{Sr}$  (Fig. 23D, E). The two modes  
401 in both wells are probably equivalent. When applying the  $^{87}\text{Sr}/^{86}\text{Sr}$ -time curve of seawater from  
402 McArthur et al. (2001), the two modes correspond to 5.5-7.5 Ma and 1.5-3 Ma, respectively (Fig.  
403 23). These two dolomitizing phases are consistent with previously suggested phase I (late  
404 Miocene) and phase II (late Pliocene) dolomitization of the Cayman Formation on Cayman  
405 Islands (Jones and Luth, 2003b; Zhao and Jones, 2012). The unimodal distribution of  $^{87}\text{Sr}/^{86}\text{Sr}$   
406 from the interior dolostones in the upper 20 m of well FFM-1, with a narrow range of 0.70906 to  
407 0.70910 may indicate phase II dolomitization alone (Fig. 23F).

408 Collectively, the available information suggests that phase I dolomitization was  
409 restricted to the coastal areas of the island, whereas phase II dolomitization extended into the  
410 center of the island. This model is consistent with Jones and Luth (2003b, their Fig. 15) who  
411 suggested that phase I produced a patchy distribution of dolostone throughout the Cayman  
412 Formation whereas phase II resulted in dolomitization of the remaining limestone.

413 The coexistence of LCD and HCD dolomites in Cayman Formation cannot be equated  
414 with the two phases of dolomitization because both LCD and HCD were probably generated

415 during each phase. This is based on the fact that the  $^{87}\text{Sr}/^{86}\text{Sr}$  ratio cannot be related to  
416 the %LCD or %Ca in the dolomite (Fig. 24) and many crystals that have three or more  
417 alternating LCD and HCD zones. It seems improbable that each zone would represent a different  
418 phase of dolomitization.

419 Some dolomite in the Cayman Formation was diagenetically modified after each episode  
420 of dolomitization. Since the last phase of dolomitization, for example, the rapid and dramatic  
421 glacioeustatic fluctuations in sea level and subaerial exposure led to the formation of hollow  
422 dolomite crystals (Ren and Jones, 2016) and the development of inside-out dolomite (Jones,  
423 2007).

## 424 *5.2. Properties of dolomitizing fluids*

425 The Mg needed for dolomitizing the limestones in the Cayman Formation was most  
426 probably derived from seawater that surrounded Grand Cayman. Previous studies on  
427 dolomitization of the Cayman Formation on Grand Cayman and Cayman Brac concluded that  
428 seawater or slightly modified seawater mediated dolomitization (Pleydell et al., 1990; Jones and  
429 Luth, 2002; Zhao and Jones, 2012). The contrasts in the degree of dolomitization and the  
430 variations in the %Ca and HCD and LCD ratios of dolomites from the coast to the center of the  
431 island, however, may point to geographical variability in the composition of the dolomitizing  
432 fluids across the island.

### 433 *5.2.1. Evidence from carbon isotopes*

434 The  $\delta^{13}\text{C}$  values of most dolomites from the Cayman Formation (+0.52 to +3.83‰,  
435 average =  $2.37 \pm 0.84\%$ , n=206) are typical of replacive island dolostones that are generally  
436 between +0.5‰ and +3.2‰ (cf., Budd, 1997). These carbon isotopic values, as suggested by  
437 Land (1992) and Budd (1997), were largely inherited from their precursor carbonates that

438 contained marine carbon. The average  $\delta^{13}\text{C}$  difference between the coexisting dolomite and  
439 calcite in the Cayman Formation ( $\Delta^{13}\text{C}_{\text{dol-pres cal}}$ ) of about 0.6‰ (Fig. 22B) agrees with Land  
440 (1992) who argued that dolomite has < 1‰ difference in  $\delta^{13}\text{C}$  from the precursor sediment. The  
441 true fractionation between the dolomites and their precursor carbonate ( $\Delta^{13}\text{C}_{\text{dol-orig cal}}$ ) from  
442 Cayman Formation is probably < 0.6‰ because the present-day calcites that coexist with the  
443 dolomite have evolved through meteoric diagenesis after dolomitization and thus may have a  
444 lower  $\delta^{13}\text{C}$  than their precursor carbonates.

445         Although the  $\delta^{13}\text{C}$  in the dolomite may provide little information about the nature of the  
446 dolomitizing fluid that affected the Cayman Formation, some clues can still be determined by  
447 considering the spatial distribution of those values and by considering them together with the  
448 oxygen isotopes. In this respect, the following points are important:

- 449         (1) The  $\delta^{13}\text{C}$  values are related to location, with the lower values (< 2‰) being mostly from the  
450             central part of the island (dolomites in interior dolostone and limestone) and the higher  
451             values (>3‰) from the peripheral dolostones (Fig. 18A, B).
- 452         (2) Samples with a positive correlation between the  $\delta^{18}\text{O}$  and  $\delta^{13}\text{C}$  all came from the central  
453             part of the island (Fig. 19). This relationship is not apparent in the dolomite from the  
454             coastal areas. Covariation between the oxygen and carbon isotopes of carbonate is  
455             commonly regarded as an indicator of diagenetic alteration in the marine-meteoric mixing  
456             zone (e.g., Allan and Matthews, 1982). In this zone, both isotopes in the water increase  
457             with depth from typical meteoric values to marine values. The positive covariation  
458             between  $\delta^{18}\text{O}$  and  $\delta^{13}\text{C}$  evident in dolomites from the Yucatan Peninsula was attributed to a  
459             mixing zone origin (Ward and Halley, 1985). The positive  $\delta^{13}\text{C}$  values, along with the

460 covariation between  $\delta^{13}\text{C}$  and  $\delta^{18}\text{O}$  of the dolomites from the interior of Cayman Island  
461 indicate that they were probably precipitated in the lower part of the mixing zone.

462 Together, these points indicate that the dolomitizing fluids in the peripheral and interior  
463 parts of the island were different. Assuming that the dolomitizing fluid of the peripheral  
464 dolostones was seawater, the above points indicate that the parent fluid of the interior dolostone  
465 and limestone was probably a mixture of (modified) seawater and meteoric water.

#### 466 5.2.2. *Evidence from oxygen isotopes*

467 Factors that determine the  $\delta^{18}\text{O}$  value of dolomite include primarily reaction temperature  
468 and the  $\delta^{18}\text{O}$  of the dolomitizing fluid (Land, 1985), dolomite stoichiometry (Aharon et al., 1987;  
469 Vahrenkamp et al., 1994; Gill et al., 1995; Zhao and Jones, 2012), dolomite precipitation rates  
470 (Vahrenkamp et al., 1994), and phosphoric acid fractionation (Aharon et al., 1977; Land and  
471 Moore, 1980). The role of non-stoichiometry on  $\delta^{18}\text{O}$  values is evident in many Cenozoic  
472 dolostones. As yet, however, no agreement has been reached on the rate at which the  $\delta^{18}\text{O}$   
473 changes relative to the %Ca of the dolomite. Proposed values per 1% increase in the %Ca  
474 include -0.1‰ (the Bahamas; Vahrenkamp et al., 1994), -0.33‰ (St. Croix; Gill et al., 1995), -  
475 0.2‰ (Niue; Wheeler et al., 1999), -0.15‰ (Kita-daito-jima; Suzuki et al., 2006), and -0.26‰  
476 (Cayman Brac; Zhao and Jones, 2012). Budd (1997) suggested that the correction proposed by  
477 Vahrenkamp et al. (1994), of about -0.1‰, was probably the most realistic.

478 Data from the dolomites in the Cayman Formation examined in this study gives rise to  
479 the following values for the rate of change between  $\delta^{18}\text{O}$  and %Ca:

480 (1) -0.34‰ – based on all dolomite samples, irrespective of their %Ca (Fig. 20A).

481 (2) -0.15‰ – based on dolomite samples with >90%LCD (Fig. 20C).

482 (3) -0.19‰ – based on dolomite samples with >90%HCD (Fig. 20D).

483           The low correlations between the  $\delta^{18}\text{O}$  and average %Ca in the above three plots ( $r^2 = 0.40$ ,  
484 0.03, 0.60, respectively) indicate that factors (e.g., dolomitizing fluid, reaction rate) other than  
485 non-stoichiometry have affected the oxygen isotopes (cf., Vahrenkamp et al., 1994; Wheeler et  
486 al., 1999). The rate based on the plot of all dolomites (0.34‰) is much higher than those  
487 suggested for many other island dolostones. This higher  $\delta^{18}\text{O}_{\text{dol}}-\text{\%Ca}$  rate can probably be  
488 attributed to the dolomitizing fluid rather than stoichiometry. As noted previously (Figs. 13-16),  
489 most HCD-dominated samples come from the island interior whereas LCD-dominated samples  
490 came from the periphery. The  $\delta^{18}\text{O}$  values of the dolomitizing fluid probably varied in different  
491 areas and this would have affected the  $\delta^{18}\text{O}$  of the dolomites and thus exaggerated the slope of  
492 the regression line between  $\delta^{18}\text{O}$  and %Ca.

493           The stratigraphic trend of the oxygen isotopes also shows that dolomite stoichiometry had  
494 less influence than other factors. Dolostones in the upper part of many wells commonly have  
495 lower  $\delta^{18}\text{O}$  values than those at the base (Fig. 21). In every well, the increase in  $\delta^{18}\text{O}$  with depth  
496 (Fig. 21), which is independent of the %Ca, may indicate that (1) the influence of %Ca on the  
497  $\delta^{18}\text{O}$  is not as significant as previously suggested (e.g., Vahrenkamp et al., 1994; Zhao and  
498 Jones; 2012), (2) post-dolomitization diagenesis of the dolostones may have modified their  
499 isotopes, (3) dolostones at depth may have formed during sea-level lowstands when seawater  
500 was probably more enriched with  $^{18}\text{O}$  than during the highstands (cf., Chappell and Shackleton,  
501 1986), and/or (4) the dolomite pore-water temperature is lower at depth than at the surface and  
502 there is a gradual decreasing of the temperature with depth.

503           Given that there are still uncertainties over the non-stoichiometric effect on dolomite  
504  $\delta^{18}\text{O}$  values, as well as the phosphoric acid fractionation factor (Land and Moore, 1980;

505 Rosenbaum and Sheppard, 1986; Vahrenkamp et al., 1994; Zhao and Jones, 2012), the raw  $\delta^{18}\text{O}$   
 506 data derived from the Cayman dolomites were not corrected for these two factors.

507 Equation (1), developed by Land (1985), can be used to estimate the  $\delta^{18}\text{O}$  of the  
 508 dolomitizing fluid:

$$509 \quad \delta^{18}\text{O}_{\text{dolomite}} - \delta^{18}\text{O}_{\text{water}} = 1000 \ln \alpha_{\text{dolomite-water}} = 2.78(10^6 T^{-2}) + 0.91 \quad (1)$$

510 The  $\delta^{18}\text{O}_{\text{dolomite}}$  and  $\delta^{18}\text{O}_{\text{water}}$  are in SMOW, and T is in Kelvin.

511 Herein, calculations of the paleo-temperature during dolomitization were based on (1) an  
 512 average annual surface ocean water T around Cayman today of  $\sim 28^\circ\text{C}$  (capeweather.com), (2)  
 513 the assumption that there was no significant difference in the sea surface T during phases I and II  
 514 dolomitization (cf., O'Brien et al., 2014), (3) the average T gradient for groundwater was about -  
 515  $2.5^\circ\text{C}/100\text{ m}$  below 10 m bsl, and  $-2^\circ\text{C}/10\text{ m}$  from sea level to 10 m bsl, as it is today (Fig.  
 516 25D), (4) groundwater T, at any given depth, being  $\sim 1.5^\circ\text{C}$  lower in the interior than the  
 517 periphery of the island (Fig. 25D), and (5) during phase I dolomitization, sea level rose from at  
 518 least -40 m below to  $\sim 15\text{ m}$  above present sea level, and during Phase II dolomitization, sea level  
 519 rose from -40 m to at least 12.5 m above present sea level (Jones and Luth, 2003b). Accordingly,  
 520 dolomitization of the peripheral dolostones at 4 m asl to 94 m bsl interval involved fluid with T  
 521 of  $24\text{-}28^\circ\text{C}$ ; the transitional dolostone at 3 m asl to 77 m bsl in wells HRQ-3 and CKC-1 at T of  
 522  $22.5\text{-}26.5^\circ\text{C}$ ; the interior dolostone at 3 m asl to 52 m bsl in HRQ-1 and HRQ-2 at T of  $23.2\text{-}$   
 523  $24.5^\circ\text{C}$ ; and the interior limestone 52-124 m bsl in wells HRQ-1 and HRQ-2 at T of  $21.5\text{-}24.5$   
 524  $^\circ\text{C}$ . These temperatures were used to calculate the  $\delta^{18}\text{O}$  of the dolomitizing fluids ( $\delta^{18}\text{O}_{\text{water}}$ ) that  
 525 mediated the four different types of dolomites (Fig. 26).

526 (1) Peripheral dolostone – The calculated  $\delta^{18}\text{O}_{\text{water}}$  is 1.3 to 3.9‰<sub>SMOW</sub> using a  $\delta^{18}\text{O}_{\text{dol}}$  range of  
 527  $3.62 \pm 0.85$ ‰<sub>VPDB</sub> and T range of 24-28°C. The  $\delta^{18}\text{O}_{\text{water}}$  calculated from the average  
 528  $\delta^{18}\text{O}_{\text{dol}}$  (3.62‰) and T (26°C) is 2.6‰<sub>SMOW</sub>.

529 (2) Transitional dolostone – The  $\delta^{18}\text{O}_{\text{water}}$  is 0.4 to 3.1‰<sub>SMOW</sub> using a  $\delta^{18}\text{O}_{\text{dol}}$  range of  $3.10 \pm$   
 530  $0.88$ ‰<sub>VPDB</sub> and T of 22.5-26.5°C. The  $\delta^{18}\text{O}_{\text{water}}$  calculated with the average  $\delta^{18}\text{O}_{\text{dol}}$   
 531 (2.76‰) and T (24.5°C) is 1.7‰<sub>SMOW</sub>.

532 (3) Interior dolostone – The  $\delta^{18}\text{O}_{\text{water}}$  is 0.2 to 1.6‰<sub>SMOW</sub> using a  $\delta^{18}\text{O}_{\text{dol}}$  range of  $2.37 \pm$   
 533  $0.55$ ‰<sub>VPDB</sub> and T of 23.2-24.5°C. The  $\delta^{18}\text{O}_{\text{water}}$  calculated with the average  $\delta^{18}\text{O}_{\text{dol}}$   
 534 (2.37‰) and T (23.9°C) is 0.9‰<sub>SMOW</sub>.

535 (4) Interior limestone – The  $\delta^{18}\text{O}_{\text{water}}$  is -0.97‰ to 1.80‰<sub>SMOW</sub> using a  $\delta^{18}\text{O}_{\text{dol}}$  range  $2.10 \pm$   
 536  $1.03$ ‰<sub>VPDB</sub> and T of 21.5-24.5 °C. The  $\delta^{18}\text{O}_{\text{water}}$  calculated with the average  $\delta^{18}\text{O}$  (2.1‰)  
 537 and T (23°C) is 0.42‰<sub>SMOW</sub>.

538 The highest  $\delta^{18}\text{O}_{\text{water}}$  value (2.6‰<sub>SMOW</sub>), associated with the peripheral dolostone,  
 539 supports the notion that seawater mediated pervasive dolomitization in the peripheral part of the  
 540 island given that the average  $\delta^{18}\text{O}$  of seawater around Grand Cayman today is 1.06‰, and that  
 541 seawater  $\delta^{18}\text{O}$  values were probably 0.3-0.8‰ higher during the early Pliocene (Medina-Elizalde  
 542 et al., 2008) and Pleistocene (Wheeler et al., 1999). The higher calculated  $\delta^{18}\text{O}_{\text{water}}$  value is  
 543 probably related to (1) the calculation method—the high  $\delta^{18}\text{O}_{\text{water}}$  values were calculated using  
 544 the high  $\delta^{18}\text{O}_{\text{dol}}$  and T (Fig. 26), whereas in reality a large  $\delta^{18}\text{O}_{\text{dol}}$  should be more likely produced  
 545 at depth with a lower T (Fig. 21), (2) slight evaporation of the seawater, or (3) glacio-eustatic  
 546 lowstands when seawater was enriched with  $^{18}\text{O}$  (cf., Wheeler et al., 1999).

547 The lowest  $\delta^{18}\text{O}_{\text{dol}}$  and calculated  $\delta^{18}\text{O}_{\text{water}}$  of the dolomites in the interior limestone  
 548 indicates that the dolomitizing fluid was more enriched with  $^{18}\text{O}$  than seawater. The oxygen

549 isotope composition of the dolomitizing fluid may have been derived from seawater, meteoric  
550 water, or from dissolution of the precursor carbonate. If the present-day  $\delta^{18}\text{O}$  values of seawater  
551 around Grand Cayman (1.06‰<sub>SMOW</sub>) and freshwater from the East End Lens (-4.83‰<sub>SMOW</sub>; Ng,  
552 1990) are utilized, the calculated  $\delta^{18}\text{O}_{\text{water}}$  values of the fluid that mediated partial dolomitization  
553 of the limestones corresponds to a mixture of seawater with < 34% freshwater; and if the mean  
554 average of  $\delta^{18}\text{O}_{\text{water}}$  (0.42‰) is used, a mixture of 11% freshwater with seawater is indicated.  
555 This degree of mixing suggests that dolomitization in the island interior may have taken place in  
556 the lower mixing to upper saline zone, which is probably the strongest circulation zone in the  
557 marine phreatic zone (cf., Kaufman, 1994; Whitaker et al., 2004).

558         Today, the  $\delta^{18}\text{O}_{\text{water}}$  values of the saline groundwater from the interior wells are lower  
559 than those from the coastal wells (Fig. 25C). There is no correlation between the  $\delta^{18}\text{O}_{\text{water}}$  and  
560 the chloride concentration or the rock type in which it resides. This indicates that the low  $\delta^{18}\text{O}$   
561 of saline water was not introduced by meteoric water or caused by water-rock reaction. It is  
562 difficult, however, to determine the  $\delta^{18}\text{O}_{\text{water}}$  of saline groundwater when dolomitization of the  
563 central limestone took place. If the situation was like today, the  $\delta^{18}\text{O}_{\text{water}}$  would have been ~  
564 0.85‰. If so, the fluid that mediated dolomitization may have been modified seawater with  
565 depleted  $^{18}\text{O}$  rather than mixed seawater and meteoric water. The low  $\delta^{18}\text{O}_{\text{water}}$  of the saline  
566 groundwater in the island interior may have been generated by the dolomitization process itself  
567 because the heavy oxygen would have been preferentially consumed. At the island-wide scale,  
568 the  $\delta^{18}\text{O}_{\text{water}}$  of the pore fluid was almost certainly continually evolving because of rock-water  
569 reaction along the flow path from shelf edge to center of the island. This may also explain the  
570 decreasing trend of  $\delta^{18}\text{O}_{\text{water}}$  of the dolomitizing fluids that led to the formation of the peripheral

571 dolostone, to the transitional dolostone, the interior dolostone and to dolomites in the interior  
572 dolostone (Fig. 26).

573         The differences in the  $\delta^{18}\text{O}$  of coexisting dolomite and calcite ( $\Delta^{18}\text{O}_{\text{dol-cal}} = \delta^{18}\text{O}_{\text{dol}} -$   
574  $\delta^{18}\text{O}_{\text{pres-cal}} = 1.75 \pm 0.65\text{‰}$ ; Fig. 22A) are far less than the fractionation  $\Delta^{18}\text{O}_{\text{dol-cal}}$  that many  
575 authors have suggested (e.g., 3.8 ‰ of Land, 1991; 3‰ of Fouke, 1994; 3-5‰ of Budd, 1997).  
576 Limestones in the island interior have undergone various diagenetic modifications in meteoric  
577 settings since the last phase of pervasive dolomitization, which resulted in the reduced  $\delta^{18}\text{O}_{\text{pres-cal}}$   
578 values of the present-day calcium carbonate compared with the original sediments ( $\delta^{18}\text{O}_{\text{orig-cal}}$ )  
579 (Ren and Jones, 2016). If this is taken into consideration, the true  $\Delta^{18}\text{O}_{\text{dol-cal}}$  between the  
580 dolomites and their precursor carbonate ( $=\delta^{18}\text{O}_{\text{dol}} - \delta^{18}\text{O}_{\text{orig-cal}}$ ) would be lower than 1.75‰ and  
581 much lower than the theoretical value of 3-4‰. The low  $\Delta^{18}\text{O}_{\text{dol-cal}}$  was caused, most likely, by  
582 the decreasing of  $^{18}\text{O}_{\text{dol}}$ . This supports the notion that the dolomites that coexist with calcite  
583 (dolomite in the interior island) were formed from fluids that were, relative to seawater, depleted  
584 with respect to  $^{18}\text{O}$ .

585         Interpretations of the properties of the dolomitizing fluids based on the oxygen isotopes  
586 are consistent with those derived from the carbon isotopes. Together with variations in dolomite  
587 stoichiometry, the oxygen and carbon isotope data indicate that the (1) compositions of the  
588 dolomitizing fluids varied from the margin to the center of the island, (2) dolomitization in the  
589 peripheral areas was mediated by seawater that may have been slightly evaporated, (3) seawater  
590 gradually lost its  $^{18}\text{O}$  as it migrated towards to the island center due to the water-rock reaction  
591 (i.e., dolomitization), (4) fluids that mediated dolomite formation in the interior limestones were  
592 probably a mixture of seawater that had been modified by dolomitization, and meteoric water,

593 and (5) dissolution of the precursor carbonate may have also influenced the isotopic  
594 compositions of the dolomites.

595 As Budd (1997) pointed out, isotopic values determined from bulk-rock samples must  
596 represent an average of numerous populations of dolomite. Thus, the interpretations provided  
597 here address the general conditions of dolomitization, but cannot be specific to each generation  
598 of dolomite.

## 599 **6. Discussion**

600 Dolostones in the Cayman Formation on Grand Cayman provide an opportunity for  
601 assessing the origin of thick dolostone successions. Island dolostones like these, found on many  
602 Caribbean islands and Pacific atolls (see Budd, 1997), have attributed to many different  
603 formational models (e.g., Tucker and Wright, 1990; their Fig. 8.31), including ocean current  
604 pumping (Saller, 1984; Wheeler et al., 1999), seepage reflux (Deffeyes, 1965; Ohde and  
605 Elderfield, 1992; Lucia and Major, 1994; Gill et al., 1995), tidal pumping (Carballo et al., 1987),  
606 and Kohout convection (Aharon et al., 1987; Machel, 2000). Most of these interpretations are  
607 based largely on the large-scale geometry of the dolostone bodies, stratigraphic relationships  
608 between the coeval dolostones and limestones, and the petrographic and geochemical attributes  
609 of the dolomite (e.g., Hardie, 1987; Wilson et al., 1990; Braithwaite, 1991; Budd, 1997; Warren,  
610 2000).

611 Natural dolomite, like that in the Cayman Formation on the Cayman Islands, is a  
612 compositional series with variable Mg and Ca ratios (Lumsden and Chimahusky, 1980; Sperber  
613 et al., 1984; Land, 1985; Sibley, 1990; Vahrenkamp et al., 1994; Budd, 1997; Wheeler et al.,  
614 1999; Swart and Melim, 2000; Jones and Luth, 2002). Although deemed “important” by Land  
615 (1985), these stoichiometric variations are usually not integrated into most dolomitization models.

616 Dolostones of all ages are commonly Ca-rich with many containing two or more populations of  
617 dolomite with different %Ca. Three populations are present in the Miocene-Pliocene dolostones  
618 from Niue Island (Wheeler et al., 1999) and four populations have been identified in the  
619 dolostones from Kita-daito-jima (Suzuki et al., 2006). On the Cayman Islands, Oligocene-  
620 Pliocene dolostones are formed of LCD and/or HCD (Jones and Luth, 2002). Likewise, Ca-rich  
621 non-stoichiometric dolostones with more than one population of dolomite are also common  
622 among ancient dolostones, including those from North America that were documented by  
623 Lumsden and Chimahusky (1980) and Sperber et al. (1984). Such examples suggest that  
624 heterogeneous dolomites are universal and have been present throughout geologic history. This  
625 is a critical issue because many other geochemical attributes (e.g., stable isotopes) are known to  
626 vary in accord with the %Ca of the dolomite (e.g., Vahrenkamp et al., 1991, 1994).

627         Many field (Lumsden and Chimahusky, 1980; Sass and Bein, 1988) and laboratory  
628 (Goldsmith and Graf, 1958; Katz and Matthews, 1977; Sibley et al., 1987, 1994; Sibley, 1990;  
629 Nordeng and Sibley, 1994; Kaczmarek and Sibley, 2011, 2014) studies have shown that dolomite  
630 stoichiometry is an important indicator of the chemical properties of their formative solutions.  
631 Folk and Land (1975) argued that the formation of (near)-stoichiometric dolomites is generally  
632 associated with solutions that have high salinities and high Mg/Ca ratios. Similarly, various  
633 experiments have also demonstrated that both the composition of the synthesized dolomite and  
634 the rate of replacement are highly dependent on the Mg/Ca in the formative solutions (e.g.,  
635 Kaczmarek and Sibley, 2011).

636         On Grand Cayman, the overall trend of increasing volumes of HCD and decreasing  
637 volumes of LCD towards the island centre suggests that variations in dolomite stoichiometric  
638 were related to the landward migration of the seawater that mediated dolomitization (Fig. 27).

639 With this model, there was a progressive loss of Mg and hence a decrease in the Mg/Ca ratio as  
640 the seawater moved inland. Accordingly, while seawater mediated LCD formation in the coastal  
641 areas, HCD was formed in the transitional zone, and dolomitization did not take place in the  
642 central part of the island. This pattern indicates that the chemical composition of the pore fluids  
643 was continually evolving along its flow path due to the rock-water interaction (Fig. 27). This is  
644 comparable with the present-day hydrochemistry whereby a progressive landward decrease in  
645 the Mg/Ca ratio of the saline water is evident (Fig. 22).

646 The lateral extent of dolomitization in the Cayman Formation on Grand Cayman was  
647 controlled largely by fluxes in the Mg supply. The fact that dolomitization was mediated by  
648 laterally derived seawater excludes the seepage reflux and thermal convection models as viable  
649 mechanisms for seawater circulation through the island. Sea level lowstands before each phase  
650 of dolomitization on Grand Cayman, meant that the island was subaerially exposed. Jones and  
651 Luth (2003b) argued that karst development during these lowstands led to increased porosity and  
652 permeability in the bedrock that would, during the next transgressive phase, have enhanced  
653 groundwater circulation throughout the island. The submixing-zone circulation model was  
654 proposed as the driving mechanism for dolomitization in Barbados (Machel et al., 1990) and the  
655 Bahamas (Vahrenkamp et al., 1991, 1994). Numerical simulation models for submixing-zone  
656 flow (Kaufman, 1994; Whitaker et al., 2004), also support this assessment.

657 Whitaker et al. (2004), using a model carbonate island that was 4.5 km wide with a  
658 recharge of 0.5 m/year and a freshwater lens ~30 m thick (parameters akin to the eastern part of  
659 Grand Cayman), showed that the flow rate can be as high as  $5 \times 10^{-7}$  m/s in the coastal mixing  
660 zone. The flow and flux in the submixing-zone decreases landwards and downwards from the  
661 mixing zone (e.g., Kaufman, 1994; Whitaker et al., 2004). As illustrated in the model developed

662 by Whitaker et al. (2004, their Fig. 10), the flow draws in seawater over a zone that extends to ~  
663 1 km offshore of their 4.5 km wide model island. The reduced flow rate and restricted flux of  
664 submixing-zone flow are probably important constraints on the supply of Mg to the island  
665 interior and may account for the lack of dolomitization in that part of the island. Moreover,  
666 dolomite cements and cavity-filling sediments that are common in the peripheral dolostones (Ren  
667 and Jones, 2016) may also have reduced pore connectivity and reduced groundwater circulation  
668 that, in turn, curtailed the Mg supply.

669         The fact that the different dolostones zones are concentrically arranged on Grand Cayman  
670 supports the notion that seawater flowed into the island from all directions during dolomitization  
671 (Fig. 26). The rate and volume of flow may have varied from coast to coast in accord with local  
672 factors such as permeability in the bedrock carbonates, precipitation, climate, oceanographic  
673 currents, sea level fluctuations, platform geometry, and/or geography. Thus, the lateral extent of  
674 dolostone relative to the bordering coastline may indicate local variability in the lateral  
675 penetration of the dolomitizing fluids. On Grand Cayman, for example, the dolostones and the  
676 peripheral dolostone zone extend further inland from the northeast corner than from any other  
677 direction (Fig. 6). This suggests that the highest flux, and/or flow rate of seawater came from the  
678 northeast. This may be related to the permeability patterns in the bedrock, different topographic  
679 features, and/or a dominant paleowind direction from the northeast.

680         The dolomitization model developed for the dolostones on Grand Cayman may be  
681 applicable to Cenozoic dolostones found on other islands throughout the world. Like the Grand  
682 Cayman dolostones, the stoichiometric and geochemical attributes of the island dolostones can  
683 be used as indicators of the fluid flow directions and the source of Mg. Some caution must be  
684 used when applying this model to the interpretation of ancient dolostones, which may have

685 experienced more than one phase of dolomitization/diagenetic modification with each phase  
686 involving a different source for the reactants and different flow patterns.

687         The non-stoichiometric signature of the dolostones from Grand Cayman, as with many  
688 Cenozoic dolostones, means that they are susceptible to further diagenetic modifications. When  
689 exposed to aggressive fluids such as meteoric water, the preferential dissolution of HCD can lead  
690 to the development of hollow dolomite crystals (James et al., 1993; Jones and Luth, 2003a; Swart  
691 et al., 2005), which may be further modified to inside-out dolomites (Jones, 2007). These  
692 processes could modify the quantity of dolostones as reservoir rocks by creating or occluding  
693 porosities. When buried, recrystallization of both dolomites is very likely to happen with time,  
694 resulting in an increase in the Mg/Ca ratio and cation ordering (McKenzie, 1981; Nordeng and  
695 Sibley, 1994; Malone et al., 1996; Machel, 1997; Kaczmarek and Sibley, 2014). Whether early  
696 meteoric or late burial diagenesis, modifications of dolomites can significantly change their  
697 geochemistry (e.g., Land, 1980; Land, 1985).

## 698 **7. Conclusions**

699         A network of wells drilled on the east end of Grand Cayman allowed assessment of the  
700 spatial variations in many aspects of the subsurface dolostones. Dolomites on the island are  
701 calcium-rich and composed of LCD and HCD. The geographic variations in the attributes of the  
702 dolostones, particularly with respect to the LCD and HCD and the oxygen and carbon values,  
703 provide a unique perspective on the origin of dolostone. Analysis of Cayman dolostones has led  
704 to the following conclusions:

- 705         • The Miocene Cayman Formation is incompletely dolomitized with the peripheral zone  
706         being completely dolomitized whereas limestones are still present in the island interior.

- 707       • Based on the distribution of LCD and HCD, the Cayman Formation is divided into the  
708       peripheral dolostone zone, the transitional dolostone zone, and the interior  
709       limestone/dolostone zone. These concentrically arranged zones differ in their LCD/HCD  
710       compositions, petrographic attributes, and geochemical signatures.
- 711       • Seawater provided the Mg needed for dolomitization of the Cayman Formation.  
712       Geographic variations in these dolostones reflect modifications of seawater chemistry  
713       caused by rock-water interaction as the dolomitizing fluids moved towards the island  
714       centre.
- 715       • The Cayman Formation experienced two major phases of dolomitization as suggested by  
716        $^{87}\text{Sr}/^{86}\text{Sr}$  of the dolomites; the first during the late Miocene–early Pliocene, and the  
717       second during the late Pleistocene. Dolomitization probably took place in the submixing  
718       zone where seawater was pumped into the island from all directions.
- 719       • The Mg/Ca in the dolomites is an important proxy that could be applied in the  
720       interpreting the origin and the flow directions of dolomitizing fluid. As such it is a  
721       practical demonstration of the concept first argued by Kaczmarek and Sibley (2011) on  
722       the basis of their experimental work.

723       The model developed from dolostones on Grand Cayman is probably applicable to island  
724       dolostones throughout the world.

## 725   **Acknowledgements**

726       We are grateful to the Natural Sciences and Engineering Research Council of Canada that  
727       funded this research (grant No. ZA635 to Jones), the numerous land owners on Grand Cayman  
728       who gave permission for drilling on their land, the drilling crews from Industrial Services and  
729       Equipment Ltd. who spent long days drilling the wells, and numerous staff members from the

730 Water Authority, Cayman Islands, who helped to collect samples during drilling, Hendrik van  
731 Genderen (Water Authority) who provided considerable logistical support during the drilling  
732 program, Diane Caird who ran the XRD analyses, and Nathan Gerein who helped take the SEM  
733 photomicrographs. We are indebted to Dr. S. Kaczmarek and J. Knight who provided critical  
734 reviews of the original version of this manuscript.  
735

736

737

**References**

- 738 Aharon, P., Kolodny, Y., Sass, E., 1977. Recent hot brine dolomitization in the "Solar Lake",  
739 Gulf of Elat, isotopic, chemical, and mineralogical study. *Journal of Geology* 85, 27-48.
- 740 Aharon, P., Socki, R.A., Chan, L., 1987. Dolomitization of atolls by sea water convection flow:  
741 test of a hypothesis at Niue, South Pacific. *Journal of Geology* 95, 187-203.
- 742 Blake, D.F., Peacor, D.R., Wilkinson, B.H., 1982. The sequence and mechanism of low-  
743 temperature dolomite formation: calcian dolomites in a Pennsylvanian echinoderm. *Journal*  
744 *of Sedimentary Research* 52, 59-70.
- 745 Blanchon, P., Jones, B., 1995. Marine-planation terraces on the shelf around Grand Cayman: a  
746 result of stepped Holocene sea-level rise. *Journal of Coastal Research* 11, 1-33.
- 747 Braithwaite, C.J.R., 1991. Dolomites, a review of origins, geometry and textures. *Earth and*  
748 *Environmental Science Transactions of the Royal Society of Edinburgh* 82, 99-112.
- 749 Budd, D.A., 1997. Cenozoic dolomites of carbonate islands: their attributes and origin. *Earth-*  
750 *Science Reviews* 42, 1-47.
- 751 Carballo, J.D., Land, L.S., Miser, D.E., 1987. Holocene dolomitization of supratidal sediments  
752 by active tidal pumping, Sugarloaf Key, Florida. *Journal of Sedimentary Petrology* 57, 153-  
753 165.
- 754 Chai, L., Navrotsky, A., Reeder, R.J., 1995. Energetics of calcium-rich dolomite. *Geochimica et*  
755 *Cosmochimica Acta* 59, 939-944.
- 756 Chappell, J., Shackleton, N.J., 1986. Oxygen isotopes and sea level. *Nature* 324, 137-140.
- 757 Dawans, J.M., Swart, P.K., 1988. Textural and geochemical alternations in Late Cenozoic  
758 Bahamian dolomites. *Sedimentology* 35, 385-403.

- 759
- 760
- 761 Deffeyes, K.S., 1965. Dolomitization of recent and Plio-Pleistocene sediments by marine  
762 evaporite waters on Bonaire Netherlands Antilles. In: Pray, L.C., Murray, R.C. (Eds.),  
763 Dolomitization and Limestone Diagenesis. SEPM Special Publication 13, pp. 71-88.
- 764 Der, A., 2012. Deposition and sea level fluctuation during Miocene times, Grand Cayman,  
765 British West Indies. Unpublished M.Sc. thesis, University of Alberta, 101 pp.
- 766 Drits, V.A., McCarty, D.K., Sakharov, B., Milliken, K.L., 2005. New insight into structural and  
767 compositional variability in some ancient excess-Ca dolomite. *Canadian Mineralogist* 43,  
768 1255-1290.
- 769 Folk, R.L., Land, L.S., 1975. Mg/Ca ratio and salinity: two controls over crystallization of  
770 dolomite. *American Association of Petroleum Geologists Bulletin* 59, 60-68.
- 771 Folkman, Y., 1969. Diagenetic dedolomitization in the Albian-Cenomanian Yagur Dolomite on  
772 Mount Carmel (northern Israel). *Journal of Sedimentary Research* 39, 380-385.
- 773 Fouke, B.W., 1994. Deposition, diagenesis and dolomitization of Neogene Seroe Domi  
774 Formation coral reef limestones on Curaçao, Netherlands Antilles. *Natuurwetenschappelijke*  
775 *Studiekring voor het Caraïbisch Gebied*, Amsterdam, 182 pp.
- 776 Gill, I.P., Moore Jr, C.H., Aharon, P., 1995. Evaporitic mixed-water dolomitization on St. Croix,  
777 U.S.V.I. *Journal of Sedimentary Research* 65, 591-604.
- 778 Glover, E.D., Sippel, R.F., 1967. Synthesis of magnesium calcites. *Geochimica et Cosmochimica*  
779 *Acta* 31, 603-613.
- 780 Goldsmith, J.R., Graf, D.L., 1958. Relation between lattice constants and composition of the Ca-  
781 My carbonates. *American Mineralogist* 43, 84-101.

- 782 Gregg, J.M., Bish, D.L., Kaczmarek, S.E., Machel, H.G., 2015. Mineralogy, nucleation and  
783 growth of dolomite in the laboratory and sedimentary environment: A review.  
784 *Sedimentology* 62, 1749-1769.
- 785 Hardie, L.A., 1987. Dolomitization: a critical view of some current views. *Journal of*  
786 *Sedimentary Research* 57, 166-183.
- 787 James, N.P., Bone, Y., Kyser, T.K., 1993. Shallow burial dolomitization and dedolomitization of  
788 Mid-Cenozoic, cool-water, calcitic, deep-seal limestones, southern Australia. *Journal of*  
789 *Sedimentary Research* 63, 528-538.
- 790 Jones, B., 1989. Syntaxial overgrowths on dolomite crystals in the Bluff Formation, Grand  
791 Cayman, British West Indies. *Journal of Sedimentary Petrology* 59, 839-847.
- 792 Jones, B., 2005. Dolomite crystal architecture: genetic implications for the origin of the Tertiary  
793 dolostones of the Cayman Islands. *Journal of Sedimentary Research* 75, 177-189.
- 794 Jones, B., 2007. Inside-out dolomite. *Journal of Sedimentary Research* 77, 539-551.
- 795 Jones, B., 2013. Microarchitecture of dolomite crystals as revealed by subtle variations in  
796 solubility: Implications for dolomitization. *Sedimentary Geology* 288, 66-80.
- 797 Jones, B., Hunter, I.G., 1994. Messinian (late Miocene) karst on Grand Cayman, British West  
798 Indies; an example of an erosional sequence boundary. *Journal of Sedimentary Research* 64,  
799 531-541.
- 800 Jones, B., Hunter, I., Kyser, K., 1994a. Revised Stratigraphic nomenclature for Tertiary strata of  
801 the Cayman Islands, British West Indies. *Caribbean Journal of Science* 30, 53-68.
- 802 Jones, B., Hunter, I.G., Kyser, T.K., 1994b. Stratigraphy of the Bluff Formation (Miocene-  
803 Pliocene) and the newly defined Brac Formation (Oligocene), Cayman Brac, British West  
804 Indies. *Caribbean Journal of Science* 30, 30-51.

- 805 Jones, B., Luth, R.W., 2002. Dolostones from Grand Cayman, British West Indies. *Journal of*  
806 *Sedimentary Research* 72, 559-569.
- 807 Jones, B., Luth, R.W., 2003a. Petrography of finely crystalline Cenozoic dolostones as revealed  
808 by backscatter electron imaging: Case study of the Cayman Formation (Miocene), Grand  
809 Cayman, British West Indies. *Journal of Sedimentary Research* 73, 1022-1035.
- 810 Jones, B., Luth, R.W., 2003b. Temporal evolution of Tertiary dolostones on Grand Cayman as  
811 determined by  $^{87}\text{Sr}/^{86}\text{Sr}$ . *Journal of Sedimentary Research* 73, 187-205.
- 812 Jones, B., Luth, R.W., MacNeil, A.J., 2001. Powder X-ray diffraction analysis of homogeneous  
813 and heterogeneous sedimentary dolostones. *Journal of Sedimentary Research* 71, 790-799.
- 814 Kaczmarek, S.E., Sibley, D.F., 2011. On the evolution of dolomite stoichiometry and cation  
815 order during high-temperature synthesis experiments: an alternative model for the  
816 geochemical evolution of natural dolomites. *Sedimentary Geology* 240, 30-40.
- 817 Kaczmarek, S.E., Sibley, D.F., 2014. Direct physical evidence of dolomite recrystallization.  
818 *Sedimentology* 61, 1862-1882.
- 819 Katz, A., Matthews, A., 1977. The dolomitization of  $\text{CaCO}_3$ : an experimental study at 252-295  
820 °C. *Geochimica et Cosmochimica Acta* 41, 297-308.
- 821 Kaufman, J., 1994. Numerical models of fluid flow in carbonate platforms: implications for  
822 dolomitization. *Journal of Sedimentary Research* 64, 128-139.
- 823 Land, L.S., 1985. The origin of massive dolomite. *Journal of Geological Education* 33, 112-125.
- 824 Land, L.S., 1991. Dolomitization of the Hope Gate Formation (north Jamaica) by seawater:  
825 reassessment of mixing-zone dolomite. In: Taylor, H.P., O'Neil, J.R., Kaplan, I.R. (Eds.),  
826 *Stable Isotope Geochemistry: A Tribute to Samuel Epstein*. Geochemical Society, Special  
827 *Publication* 3, pp. 121-130.

- 828 Land, L.S. 1992. The dolomite problem: stable and radiogenic isotope clues. In: Clauer, N.,  
829 Chaudhuri, S. (Eds.), *Isotopic Signatures and Sedimentary Records*. Springer, Berlin,  
830 Heidelberg, pp. 49-68.
- 831 Land, L.S., Moore, C.H., 1980. Lithification, micritization and syndepositional diagenesis of  
832 biolithites on the Jamaican island slope. *Journal of Sedimentary Research* 50, 357-369.
- 833 Liang, T., Jones, B., 2014. Deciphering the impact of sea-level changes and tectonic movement  
834 on erosional sequence boundaries in carbonate successions: A case study from Tertiary  
835 strata on Grand Cayman and Cayman Brac, British West Indies. *Sedimentary Geology* 305,  
836 17-34.
- 837 Lucia, F.J., Major, R.P., 1994. Porosity evolution through hypersaline reflux dolomitization.  
838 Dolomites. In: Purser, B.H., Tucker, M.E., Zenger, D.L. (Eds.), *Dolomites: A Volume in  
839 Honour of Dolomieu*. International Association of Sedimentologists Special Publication 21,  
840 pp. 325-341.
- 841 Lumsden, D.N., Chimahusky, J.S., 1980. Relationship between dolomite nonstoichiometry and  
842 carbonate facies parameters. In: Zenger, D.H., Dunham, J.B., Ethington, R.L. (Eds.),  
843 *Concepts and Models of Dolomitization*. SEPM Special Publication 28, pp.123-137.
- 844 Machel, H.G., 1997. Recrystallization versus neomorphism, and the concept of 'significant  
845 recrystallization' in dolomite research. *Sedimentary Geology* 113, 161-168.
- 846 Machel, H.G., 2000. Dolomite formation in Caribbean Islands: driven by plate tectonics?!  
847 *Journal of Sedimentary Research* 70, 977-984.
- 848 Machel, H.G., 2004. Concepts and models of dolomitization: a critical reappraisal. In:  
849 Braithwaite, C.J.R., Rizzi, G., Darke, G. (Eds.), *The Geometry and Petrogenesis of*

- 850 Dolomite Hydrocarbon Reservoirs. Geological Society of London Special Publication 235,  
851 pp. 7-63.
- 852 Machel, H.G., Mountjoy, E.W., Humphrey, J.D., Quinn, T.M., 1990. Coastal mixing zone  
853 dolomite, forward modeling, and massive dolomitization of platform-margin carbonates:  
854 discussion and reply. *Journal of Sedimentary Research* 60, 1008-1016.
- 855 MacNeil, A., Jones, B., 2003. Dolomitization of the Pedro Castle Formation (Pliocene), Cayman  
856 Brac, British West Indies. *Sedimentary Geology* 162, 219-238.
- 857 Malone, M.J., Baker, P.A., Burns, S.J., 1996. Recrystallization of dolomite: an experimental  
858 study from 50-200°C. *Geochimica et Cosmochimica Acta* 60, 2189-2207.
- 859 Mather, J.D., 1971. A preliminary survey of the groundwater resources of the Cayman Islands  
860 with recommendations for their development. Institute of Geological Sciences, London, 91  
861 pp.
- 862 McArthur, J.M., Howarth, R.J., Bailey, T.R., 2001. Strontium isotope stratigraphy: LOWESS  
863 Version 3: best fit to the marine Sr-isotope curve for 0–509 Ma and accompanying look-up  
864 table for deriving numerical age. *Journal of Geology* 109, 155–170.
- 865 McKenzie, J.A., 1981. Holocene dolomitization of calcium carbonate sediments from the coastal  
866 sabkhas of Abu Dhabi, U.A.E.: a stable isotope study. *Journal of Geology* 89, 185-198.
- 867 Medina-Elizalde, M., Lea, D.W., Fantle, M.S., 2008. Implications of seawater Mg/Ca variability  
868 for Plio-Pleistocene tropical climate reconstruction. *Earth and Planetary Science Letters*  
869 269, 585-595.
- 870 Ng, K.C., 1990. Diagenesis of the Oligocene-Miocene Bluff Formation of the Cayman Islands - a  
871 petrographic and hydrogeochemical approach. Unpublished PhD thesis, University of  
872 Alberta, 344 pp.

- 873 Ng, K.C., Jones, B., 1995. Hydrogeochemistry of Grand Cayman, British West Indies -  
874 implications for carbonate diagenetic studies. *Journal of Hydrology* 164, 193-216.
- 875 Ng, K.C., Jones, B., Beswick, R., 1992. Hydrogeology of Grand Cayman, British West Indies - a  
876 karstic dolostone aquifer. *Journal of Hydrology* 134, 273-295.
- 877 Nordeng, S.H., Sibley, D.F., 1994. Dolomite stoichiometry and Ostwald's step rule. *Geochimica*  
878 *et Cosmochimica Acta* 58, 191-196.
- 879 O'Brien, C.L., Foster, G.L., Martinez-Boti, M.A., Abell, R., Rae, J.W.B., Pancost, R.D., 2014.  
880 High sea surface temperatures in tropical warm pools during the Pliocene. *Nature*  
881 *Geoscience* 7, 606-611.
- 882 Ohde, S., Elderfield, H., 1992. Strontium isotope stratigraphy of Kita-daito-jima Atoll, North  
883 Philippine Sea: implications for Neogene sea-level change and tectonic history. *Earth and*  
884 *Planetary Science Letters* 113, 473-486.
- 885 Pleydell, S.M., Jones, B., Longstaffe, F.J., Baadsgaard, H., 1990. Dolomitization of the  
886 Oligocene-Miocene Bluff Formation on Grand Cayman, British West Indies. *Canadian*  
887 *Journal of Earth Sciences* 27, 1098-1110.
- 888 Reeder, R.J., 1981. Electron optical investigation of sedimentary dolomites. *Contributions to*  
889 *Mineralogy and Petrology* 76, 148-157.
- 890 Reeder, R.J. 1991. An overview of zoning in carbonate minerals. In: Barker, C.E., Burruss, R.C.,  
891 Kopp, O.C., Machel, H.G., Marshall, D.J., Wright, P., Colburn, H.Y. (Eds.), *Luminescence*  
892 *Microscopy and Spectroscopy: Qualitative and Quantitative Applications*. SEPM Special  
893 *Publication* 25, pp. 77-82.

- 894 Ren, M., Jones, B., 2016. Diagenesis in limestone-dolostone successions after 1 million years of  
895 rapid sea-level fluctuations: A case study from Grand Cayman, British West Indies.  
896 *Sedimentary Geology* 342, 15-30.
- 897 Roberts, H.H., 1994. Reefs and lagoons of Grand Cayman. In: Brunt, M.A., Davies, J.E. (Eds.),  
898 *The Cayman Islands: Natural History and Biogeography*. Springer, Netherlands, pp. 75-104.
- 899 Rosenbaum, J., Sheppard, S.M.F., 1986. An isotopic study of siderites, dolomites and ankerites  
900 at high temperatures. *Geochimica et Cosmochimica Acta* 50, 1147-1150.
- 901 Saller, A.H., 1984. Petrologic and geochemical constraints on the origin of subsurface dolomite,  
902 Enewetak Atoll: an example of dolomitization by normal seawater. *Geology* 12, 217-220.
- 903 Sass, E., Bein, A., 1988. Dolomites and salinity: a comparative geochemical study. In: Shukla,  
904 V., Baker, P.A. (Eds.), *Sedimentology and Geochemistry of Dolostones*. SEPM Special  
905 Publication 43, pp. 223-233.
- 906 Schmidt, V., 1965. Facies, diagenesis, and related reservoir properties in the Gigas Beds (Upper  
907 Jurassic), northwestern Germany. In: Prey, L.C., Murray, R.C. (Eds.), *Dolomitization and*  
908 *Limestone Diagenesis*. SEPM Special Publication 13, pp. 124-169.
- 909 Searl, A., 1994. Discontinuous solid solution in Ca-rich dolomites: the evidence and implications  
910 for the interpretation of dolomite petrographic and geochemical data. In: Purser, B.H.,  
911 Tucker, M.E., Zenger, D.L. (Eds.), *Dolomites: A Volume in Honour of Dolomieu*.  
912 International Association of Sedimentologists Special Publication 21, pp. 361-376.
- 913 Sibley, D.F., 1990. Unstable to stable transformations during dolomitization. *Journal of Geology*  
914 98, 739-748.
- 915 Sibley, D.F., Dedoes, R.E., Bartlett, T.R., 1987. Kinetics of dolomitization. *Geology* 15, 1112-  
916 1114.

- 917 Sibley, D.F., Nordeng, S.H., Borkowski, M.L., 1994. Dolomitization kinetics of hydrothermal  
918 bombs and natural settings. *Journal of Sedimentary Research* 64, 630-637.
- 919 Sperber, C.M., Wilkinson, B.H., Peacor, D.R., 1984. Rock composition, dolomite stoichiometry,  
920 and rock/water reactions in dolomitic carbonate rocks. *Journal of Geology* 92, 609-622.
- 921 Suzuki, Y., Iryu, Y., Inagaki, S., Yamada, T., Aizawa, S., Budd, D.A., 2006. Origin of atoll  
922 dolomites distinguished by geochemistry and crystal chemistry: Kita-daito-jima, northern  
923 Philippine Sea. *Sedimentary Geology* 183, 181-202.
- 924 Swart, P.K., Cantrell, D.L., Westphal, H., Handford, C.R., Kendall, C.G., 2005. Origin of  
925 dolomite in the Arab-D reservoir from the Ghawar Field, Saudi Arabia: evidence from  
926 petrographic and geochemical constraints. *Journal of Sedimentary Research* 75, 476-491.
- 927 Swart, P.K., Melim, L.A., 2000. The origin of dolomites in Tertiary sediments from the margin  
928 of Great Bahama Bank. *Journal of Sedimentary Research* 70, 738-748.
- 929 Tucker, M.E., Wright, V.P. 1990. *Carbonate Sedimentology*. Blackwell Scientific Publications,  
930 Oxford, 482 pp.
- 931 Vahrenkamp, V.C., Swart, P.K., Purser, B., Tucker, M., Zenger, D., 1994. Late Cenozoic  
932 dolomites of the Bahamas: metastable analogues for the genesis of ancient platform  
933 dolomites. In: Purser, B.H., Tucker, M.E., Zenger, D.L. (Eds.), *Dolomites: A Volume in  
934 Honour of Dolomieu*. International Association of Sedimentologists Special Publication 21,  
935 133-153.
- 936 Vahrenkamp, V.C., Swart, P.K., Ruiz, J., 1991. Episodic dolomitization of late Cenozoic  
937 carbonates in the Bahamas: evidence from strontium isotopes. *Journal of Sedimentary  
938 Research* 61, 1002-1014.

- 939 Ward, W.C., Halley, R.B., 1985. Dolomitization in a mixing zone of near-seawater composition,  
940 late Pleistocene, northeastern Yucatan Peninsula. *Journal of Sedimentary Research* 55, 407-  
941 420.
- 942 Warren, J., 2000. Dolomite: occurrence, evolution and economically important associations.  
943 *Earth-Science Reviews* 52, 1-81.
- 944 Wheeler, C.W., Aharon, P., Ferrell, R.E., 1999. Successions of Late Cenozoic platform  
945 dolomites distinguished by texture, geochemistry, and crystal chemistry: Niue, South  
946 Pacific. *Journal of Sedimentary Research* 69, 239-255.
- 947 Whitaker, F.F., Smart, P.L., Jones, G.D., 2004. Dolomitization: from conceptual to numerical  
948 models. In: Braithwaite, C.J.R., Rizzi, G., Darke, G. (Eds.), *The Geometry and Petrogenesis*  
949 *of Dolomite Hydrocarbon Reservoirs*. Geological Society of London Special Publication  
950 235, pp. 99-139.
- 951 Wilson, E.N., Hardie, L.A., Phillips, O.M., 1990. Dolomitization front geometry, fluid flow  
952 patterns, and the origin of massive dolomite: the Triassic Latemar buildup, northern Italy.  
953 *American Journal of Science* 290, 741-796.
- 954 Zhao, H., Jones, B., 2012. Origin of “island dolostones”: A case study from the Cayman  
955 Formation (Miocene), Cayman Brac, British West Indies. *Sedimentary Geology* 243-244,  
956 191-206.

**Figure captions**

- 957
- 958 **Fig. 1.** Location and geological setting of study area. (A) Location of Grand Cayman in the  
959 Caribbean Sea. (B) Geological map showing the distribution of the Cayman Formation  
960 on Grand Cayman (modified from Jones et al., 1994a), the approximate distribution of  
961 East End Freshwater Lens on the island (modified from Ng and Jones, 1992), and  
962 location of High Rock Quarry. (C) Locations of 32 wells incorporated in this study (wells  
963 in solid red dots are the primary wells used in this study). (D) Shelf profile in  
964 northeastern corner of the island, modified from Brunt (1994). (E) Distribution of 8 wells  
965 in High Rock Quarry.
- 966 **Fig. 2.** Stratigraphic succession on Grand Cayman (modified from Jones et al., 1994a).
- 967 **Fig. 3.** Distribution of seven sedimentary facies in Cayman Formation based on this study, Der  
968 (2012) and Ren and Jones (2016).
- 969 **Fig. 4.** Profile through successions in wells LBL-1, GFN-2, FFM-1, HRQ-2, ESS-1, and HMB-1  
970 showing the spatial distribution of LCD, HCD, and calcite (Cal).
- 971 **Fig. 5.** Profile through successions in wells RTR-1, FSR-1, DTE-1, HRQ-2, CKC-1, and RWP-2  
972 showing the spatial distribution of LCD, HCD, and calcite (Cal).
- 973 **Fig. 6.** Spatial distribution of peripheral dolostone, transitional dolostone, interior dolostone, and  
974 interior limestone in the Cayman Formation on the east end of Grand Cayman.
- 975 **Fig. 7.** Thin section photomicrographs illustrating the occurrence of calcite in Cayman  
976 Formation in the upper (A–C) and the lower calcite units (D–F). All depths are below  
977 ground surface. Thin sections are impregnated with blue epoxy to highlight porosity and  
978 stained with Alizarin Red S. (A) Blocky calcite cements completely filled the pores in  
979 dolostone. GFN-2, 9.6 m. (B) Pores in dolostone lined with limpid dolomite cement and

980 partly filled with calcite (red) cement. RWP-2, 3.5 m. (C) Zoned blocky calcite cements  
 981 in cavities in dolostone. HRQ-3, 3.4 m. (D) Porous benthic foraminifera limestone.  
 982 GFN-2, 34.4 m. (E) Mudstone with planktonic forams. GFN-2, 59.1 m. (F) Limestone  
 983 with a variety of fossils. GFN-2, 91.7 m.

984 **Fig. 8.** Thin section photomicrographs of peripheral dolostones. All depths are below ground  
 985 surface. (A) Fabric retentive dolostone with limpid dolomites lining the cavities. RWP-2,  
 986 94.6 m. (B) Benthic foraminifera with original fabrics well preserved in dolostone.  
 987 Chamber of the foraminifera and the intra-particle pores are lined with limpid dolomite  
 988 cement. RWP-2, 51.8 m. (C) Bladed dolomite cement encrusting grains in fabric retentive  
 989 dolostone. RWP-2, 22.0 m. (D) Fabric retentive dolostone with a complete *Halimeda*  
 990 plate, red alage fragments, and other grains. Tubules in the *Halimeda* plate and the intra-  
 991 particle pores have been filled with dolomite cement. RTR-1, 116.6 m. (E) Dolostone  
 992 with limpid dolomite filling cavities in a coral(?). RTR-1, 11.4 m. (F) Hollow dolomite  
 993 crystals with leached cores – suggesting that the dolomite crystals originally had a HCD  
 994 core. RTR-1, 130.3 m.

995 **Fig. 9.** Thin section photomicrographs of transitional dolostones (A–C), interior dolostone (D)  
 996 and dolomites in interior limestone (E, F). All depths are below ground surface. Thin  
 997 sections are impregnated with blue epoxy to highlight porosity and stained with Alizarin  
 998 Red S. (A) Dolostone with original fabrics of precursor carbonate partly preserved. HRQ-  
 999 3, 46.1 m. (B) Fabric destructive dolostone. Note molds formed by dissolution of  
 1000 foraminifera(?) in precursor carbonate. HRQ-3, 59.8 m. (C) Dolostone with original  
 1001 fabrics largely destroyed. HRQ-3, 79.6 m. (D) Fabric destructive dolostone with  
 1002 scattered limpid dolomite and blocky calcite cements. GFN-2, 2.6 m. (E, F) dolomite

1003 crystals in chambers of foraminifera in dolomitic limestone. Dissolution and fossil moldic  
 1004 porosity are common. (E) GFN-2, 7.8 m; (F) GFN-2, 7.1 m.

1005 **Fig. 10.** SEM photomicrographs of dolostones from Cayman Formation. A, C, D are etched (in  
 1006 HCl for 12 s) and polished thin sections. B is fractured surface, unetched. All depths are  
 1007 below ground surface. (A) Calcite cement filling in cavities and coating the surface of a  
 1008 red alage fragment, g=grain, cal=calcite, dol=dolomite. EER-1, 2.7 m. (B) Dolomite  
 1009 cement encrusting surface of a tubular skeletal grain held in a dolomite matrix. HRQ-5,  
 1010 4.2 m. (C) Dolomitized coral (?) with dolomite cement lining the cavities. HRQ-2,  
 1011 11.8m. (D) Distribution of dark-gray LCD (L) and light-gray HCD (H) in dolostone. Note  
 1012 open pores lined with LCD. HRQ-2, 2.7m.

1013 **Fig. 11.** SEM photomicrographs illustrating the compositional heterogeneity of dolomites from  
 1014 Cayman Formation. Polished thin sections, etched with HCl for 12 s. All from well HRQ-  
 1015 2. All depths are below ground surface. (A) Dolostone with dolomitized foraminifera,  
 1016 and dolomite cement in the pores. 42.3 m. (B) Enlarged view of etching in the matrix  
 1017 dolomites and the cement crystals in panel A. 42.3 m. (C) Enlarged view of cement  
 1018 crystal from panel B. Hollow dolomite crystal, formed by preferential dissolution of the  
 1019 core, partly refilled by dolomite cement. 42.3 m. (D) Preferential dissolution of matrix  
 1020 dolomites. 24.0 m. (E) Dolomite matrix crystals show extensive etching, and dolomite  
 1021 cements that overgrow on matrix crystals show clear zones. 8.8 m. (F) Dolomite crystals  
 1022 showing growth zones with HCD zones have been dissolved. 36.2 m. (G) Cement  
 1023 crystals showing growth zones, cortical boundaries, etch pits, and dissolution slots. 11.8  
 1024 m. (H) Dolomite crystal showing clearly defined growth zones and cortical boundaries,  
 1025 2.7 m. (I) Dolomite cement crystals with the core cut by dissolution slots. 21.0 m.

- 1026 **Fig. 12.** Distribution of LCD (low calcium dolomite), HCD (high calcium dolomite), and Cal  
1027 (calcite) in 8 wells in the Cayman Formation in High Rock Quarry (HRQ). Note similar  
1028 patterns among the closely spaced wells.
- 1029 **Fig. 13.** Distribution of LCD, HCD, and calcite (Cal) in 7 wells in the peripheral dolostone zone.  
1030 Pie charts showing the average compositions (%LCD, %HCD, and %calcite) of all  
1031 samples in each well. Histograms illustrating the %LCD in dolomite samples in each  
1032 well.
- 1033 **Fig. 14.** Distribution of LCD, HCD, and calcite (Cal) in 4 wells located in the transitional  
1034 dolostone zone. Pie charts showing the average compositions (%LCD, %HCD, and  
1035 %calcite) of all samples in each well. Histograms illustrating the %LCD in dolomite  
1036 samples in each well.
- 1037 **Fig. 15.** Distribution of LCD, HCD, and calcite (Cal) in 8 wells in the interior dolostone zone.  
1038 Pie charts showing the average compositions (%LCD, %HCD, and %calcite) of all  
1039 samples in each well. Histograms illustrating the %LCD in dolomite samples in each  
1040 well. See Fig. 6 for the distribution of the interior dolostone zone, and the locations of  
1041 wells FFM-1 and GFN-2.
- 1042 **Fig. 16.** Histograms illustrating the %LCD in dolomites in the limestone samples from each well  
1043 in the interior limestone zone. See Fig. 6 for the distribution of the interior limestone  
1044 zone, and the locations of wells FFM-1 and GFN-2.
- 1045 **Fig. 17.** Histograms of %LCD in all dolomites from (A) peripheral dolostone, (B) transitional  
1046 dolostone, (C) interior dolostone, and (D) interior limestone. Note the increase in the  
1047 frequency of the pure HCD and HCD dominated dolomites in the transitional dolostone  
1048 zone relative to the interior dolostone zone.

1049 **Fig. 18.** Oxygen and carbon isotopes of dolomites in the Cayman Formation. (A) Cross-plots of  
1050  $\delta^{18}\text{O}$  and  $\delta^{13}\text{C}$  of dolomites from all dolomite samples grouped by the peripheral  
1051 dolostone, transitional dolostone, interior dolostone, and interior limestone zones. (B)  
1052 Distribution of the average  $\delta^{18}\text{O}$  and  $\delta^{13}\text{C}$  of dolomites from the peripheral dolostone  
1053 (PD), transitional dolostone (TD), interior dolostone (ID), and interior limestone (IL)  
1054 zones (error bars represent  $\pm 1\sigma$ ). Note the decreasing trends of the isotopes from the  
1055 periphery to the interior of the island. (C) Histograms of  $\delta^{18}\text{O}$  and  $\delta^{13}\text{C}$  of dolomites from  
1056 transitional dolostone (TD) and interior dolostone (ID).

1057 **Fig. 19.** Cross-plots of  $\delta^{18}\text{O}$  and  $\delta^{13}\text{C}$  of dolomites from wells (A) CKC-1, (B) HRQ-3, and (C)  
1058 HRQ-2 showing the positive correlation between the isotopes.

1059 **Fig. 20.** Relationship between the stable isotopes and stoichiometry of the dolomite from  
1060 Cayman Formation. (A) Comparison of  $\delta^{18}\text{O}$  and average %Ca of dolomite. (B)  
1061 Comparison of  $\delta^{13}\text{C}$  and average %Ca of dolomite. (C) Comparison of  $\delta^{18}\text{O}$  and average  
1062 %Ca in dolostones with %LCD > 90%, and dolostones with %HCD > 90%.

1063 **Fig. 21.** Stratigraphic variations of  $\delta^{18}\text{O}$  and  $\delta^{13}\text{C}$  in dolostones from wells (A) RWP-2, (B)  
1064 EEZ-1, (C) LBL-1, (D) HRQ-3, (E) CKC-1, (F) HMB-1, (G) HRQ-1, and (H) HRQ-2.

1065 **Fig. 22.** Stratigraphic variations and correlations of (A)  $\delta^{18}\text{O}$  and (B)  $\delta^{13}\text{C}$  between coexisting  
1066 dolomites and calcites from well HRQ-2. Arrows showing the stratigraphic trends in the  
1067  $\delta^{18}\text{O}$  and  $\delta^{13}\text{C}$  values.

1068 **Fig. 23.** Histograms of  $^{87}\text{Sr}/^{86}\text{Sr}$  of dolostones and limestones from Cayman Formation. (A) All  
1069 dolostones from wells illustrated in B-F, and (dolomitic) limestones from wells HRQ-2,  
1070 FFM-1 and GFN-2. (B) Dolostones from well RWP-2. (C) Dolostones from well RTR-1.  
1071 (D) Dolostones from well HMB-1. (E) Dolostones from well CKC-1. (F) Dolostones

1072 from well FFM-1. (G) Two phases of dolomitization derived from  $^{87}\text{Sr}/^{86}\text{Sr}$  of dolostones  
1073 from wells B-F. Seawater  $^{87}\text{Sr}/^{86}\text{Sr}$  curve modified from McArthur et al. (2001).

1074 **Fig. 24.** Comparison of  $^{87}\text{Sr}/^{86}\text{Sr}$  with (A) %LCD in dolomite, and (B) the average %Ca of  
1075 dolomite.

1076 **Fig. 25.** Geochemistry (A-C) and temperature (D) of present-day pore water in Cayman  
1077 Formation. (A) Molar Mg/Ca ratio. (B) The contents of Mg and Ca. (C)  $\delta^{18}\text{O}$  (‰)  $\text{SMOW}$ .  
1078 (D) Temperature. Dashed lines in (A)-(C) represent the average values of 3 seawater  
1079 samples collected in Spotts Bay (south coast).

1080 **Fig. 26.** Interpretation of  $\delta^{18}\text{O}_{\text{water}}$  that mediated dolomitization of peripheral dolostones,  
1081 transitional dolostones, interior dolostones, and dolomites in interior limestone in  
1082 Cayman Formation. For each type of dolostone (dolomites), the box represent mean value  
1083  $\pm 1\sigma$ , the midline represents the mean value of  $\delta^{18}\text{O}_{\text{dol}}$ , and the solid dot represents the  
1084 calculated  $\delta^{18}\text{O}_{\text{water}}$  using mean  $\delta^{18}\text{O}_{\text{dol}}$  and temperature.

1085 **Fig. 27.** Schematic diagram of the dolomitization model on Grand Cayman. (A) 3-D view of  
1086 Cayman Formation on the east end of the island showing the concentric zones of  
1087 dolostones and limestones which indicate that seawater flowed from all directions into  
1088 the island during the dolomitization. (B) A N-S profile showing the spatial variations in  
1089 many attributes of dolostones and a variety of dolomitizing conditions from the periphery  
1090 to the interior of the island.

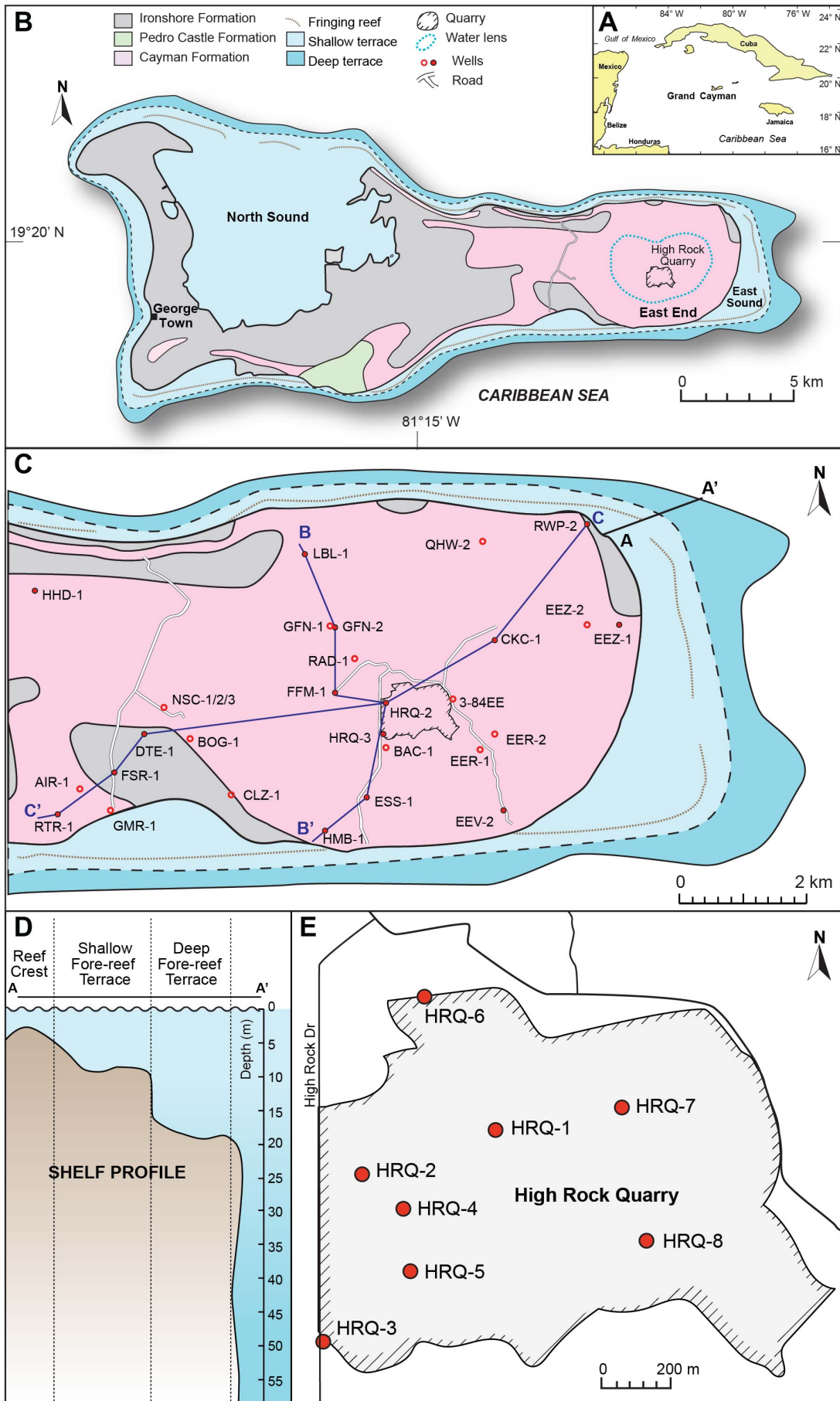


Fig. 1

AGE	UNIT	LITHOLOGY	FAUNA
HOL.		Swamp deposits storm deposits	
PLEIST.	<i>Unconformity</i> <b>IRONSHORE FORMATION</b>	Limestone	Corals (VC) Bivalves (VC) Gastropods (C)
PLIOCENE	<i>Unconformity</i> <b>PEDRO CASTLE FORMATION</b>	Dolostone (fabric retentive) and limestone	Forams (VC) Corals (C) Bivalves (LC) Gastropods (C) Red algae (C) <i>Halimeda</i> (R)
M. MIOCENE	<i>Unconformity</i> <b>CAYMAN FORMATION</b>	Dolostone (fabric retentive) and limestone locally	Corals (VC) Bivalves (LC) Rhodoliths (LC) Gastropods (R) Red algae (LC) Foraminifera (LC) <i>Halimeda</i> (R)
L. OLIG.	<i>Unconformity</i> <b>BRAC FORMATION</b>	Limestone or sucrosic dolostone (fabric destructive) with pods of limestone	Bivalves (VC) Gastropods (C) Foraminifera (VC) Red algae (R)

 limestone	 dolostone	 swamp deposits	VC=very common; C=common; LC=locally common; R=rare.
---	---	--	---

Fig. 2

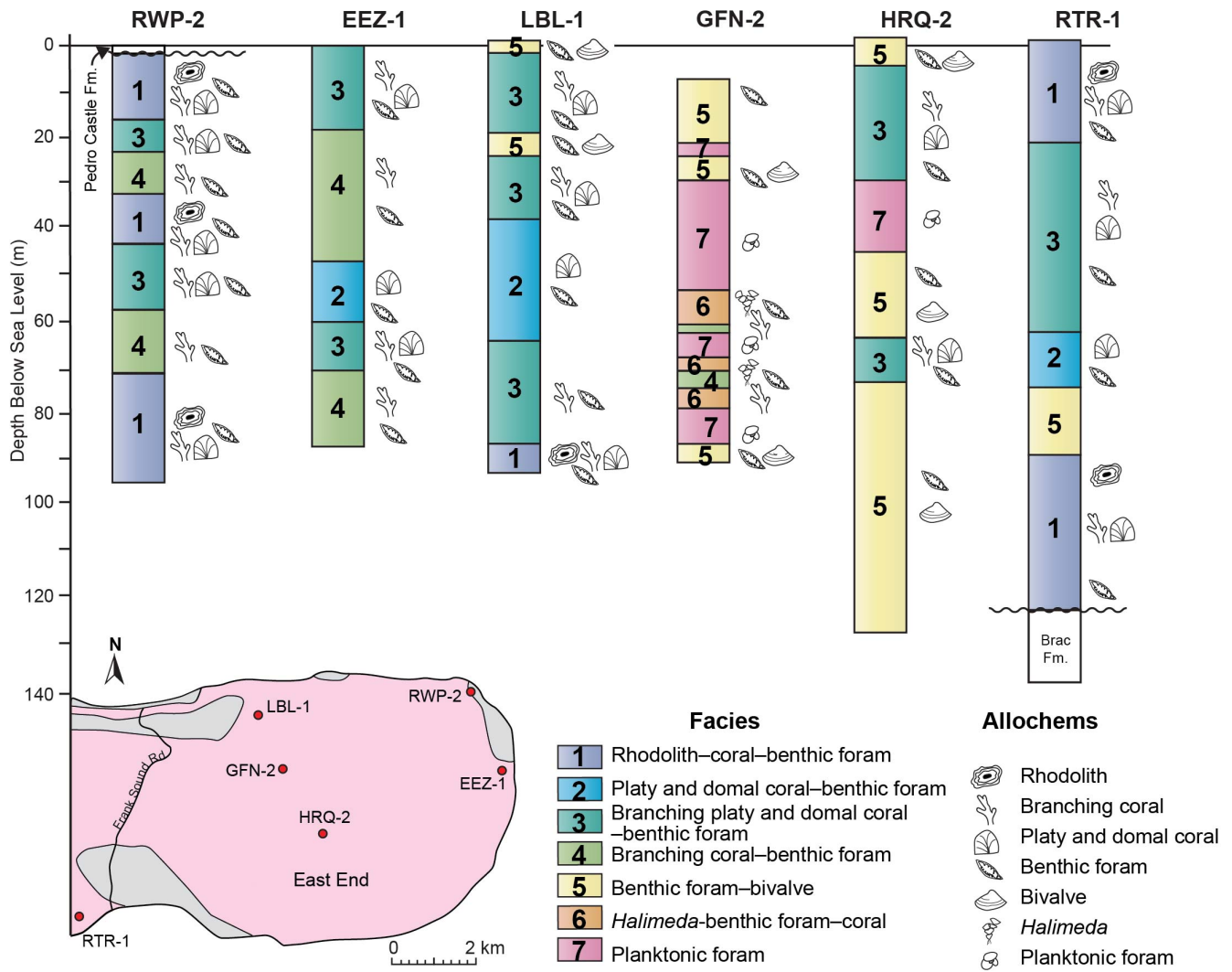


Fig. 3

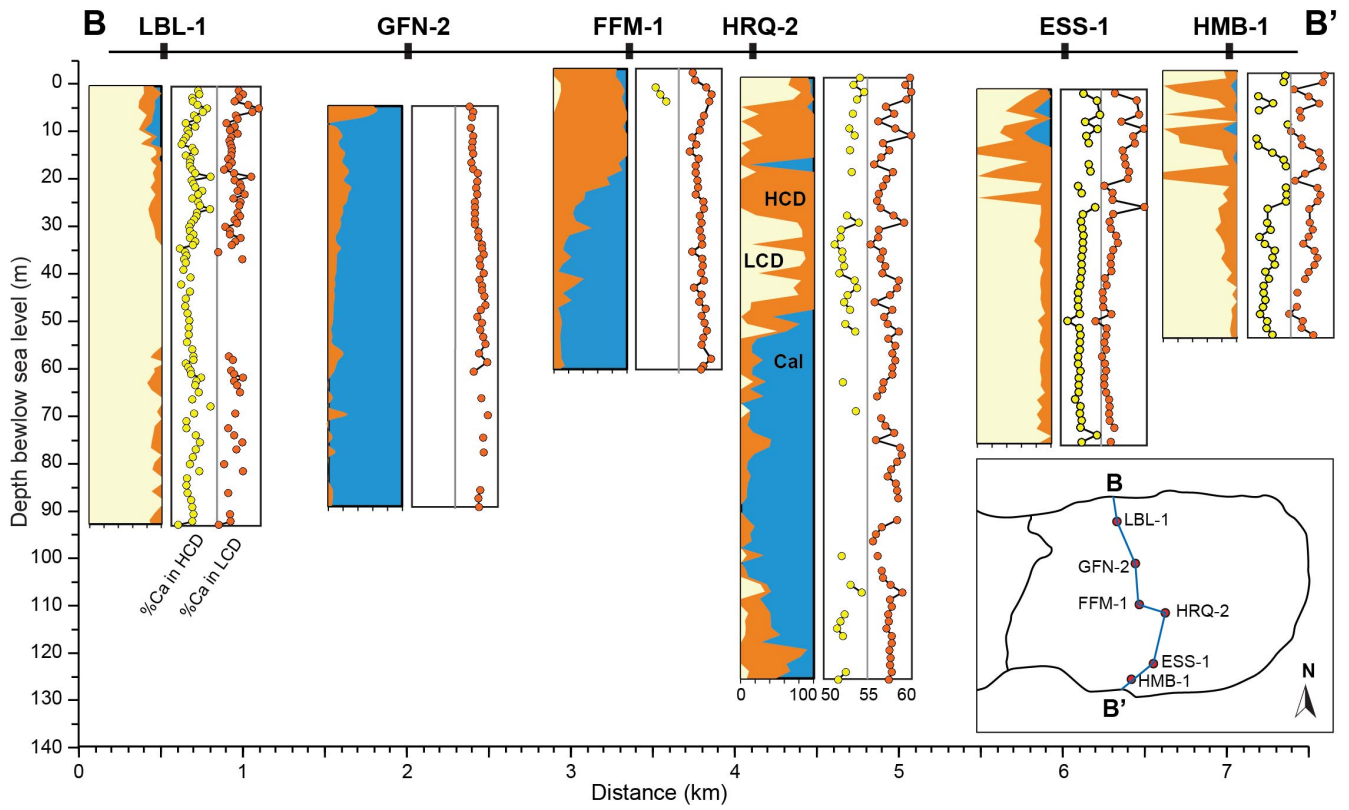


Fig. 4

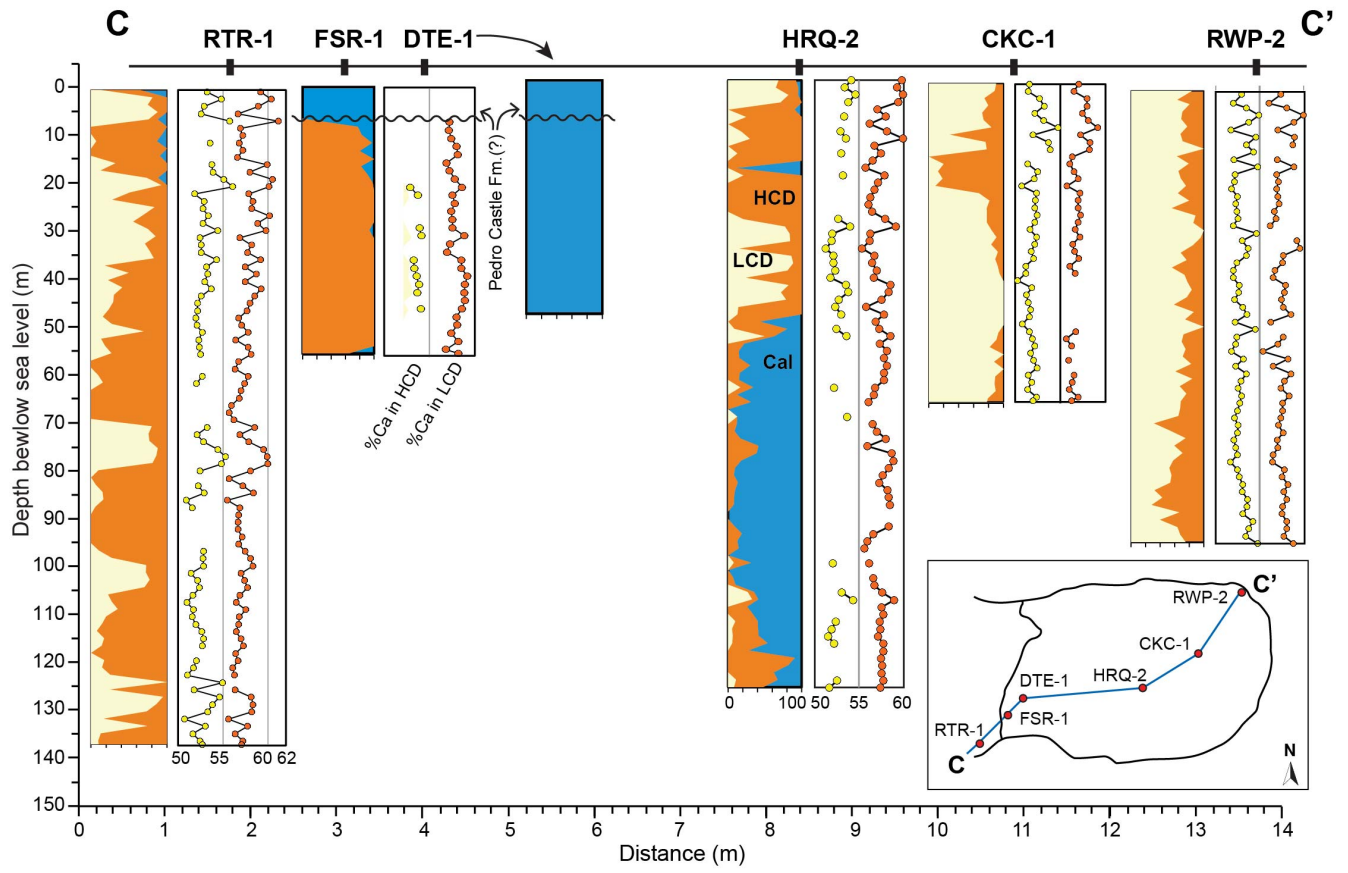


Fig. 5

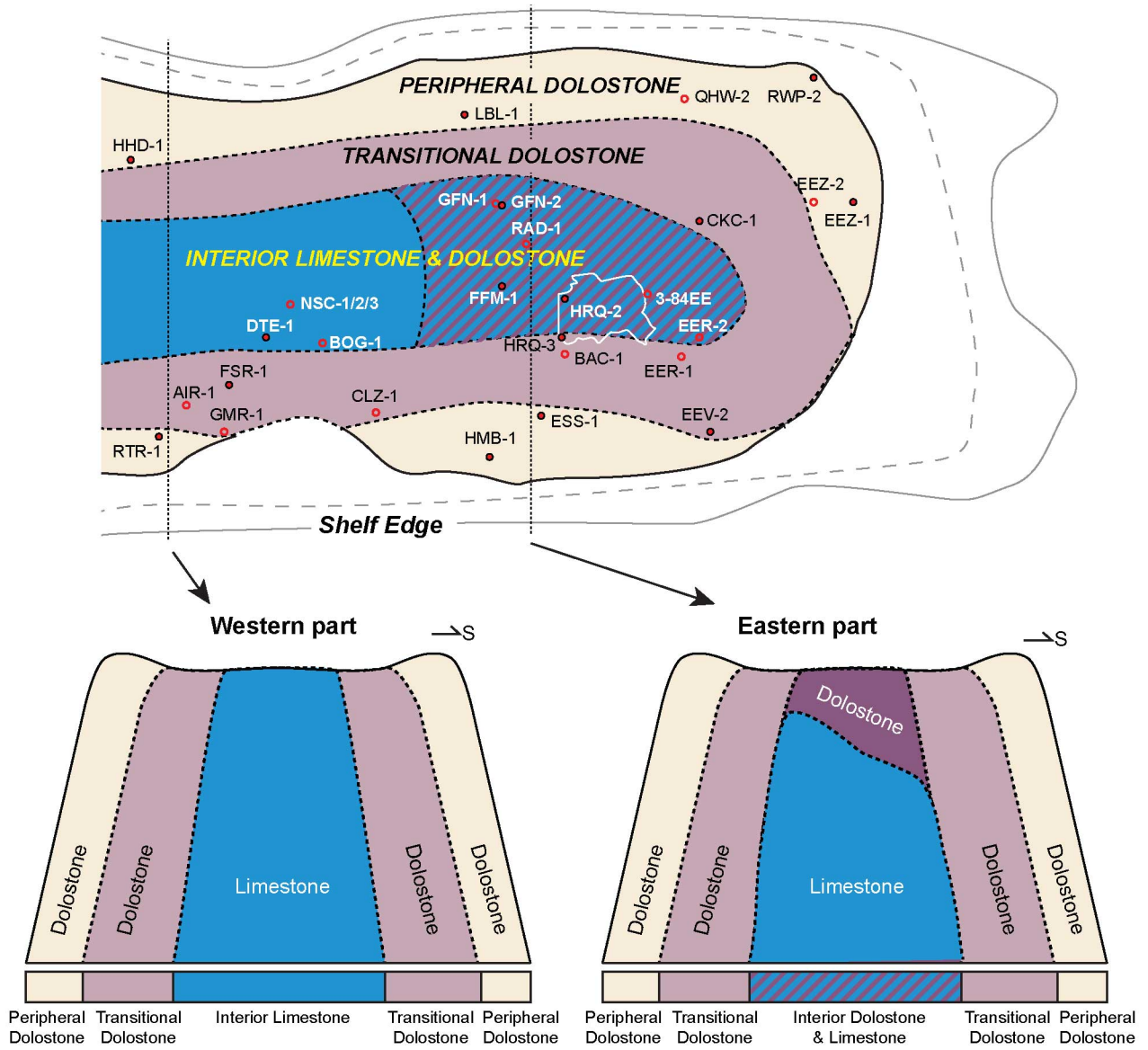


Fig. 6

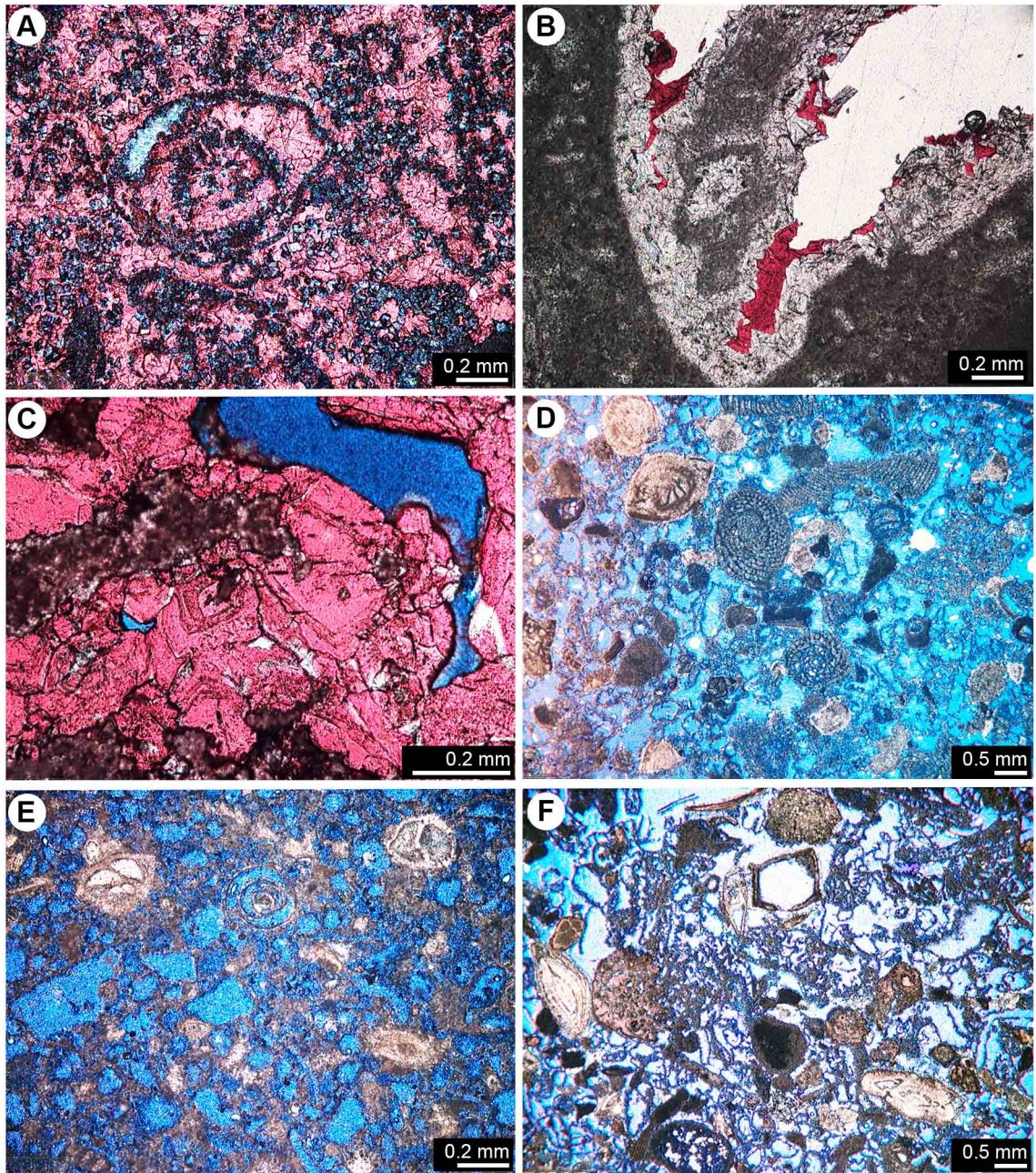


Fig. 7

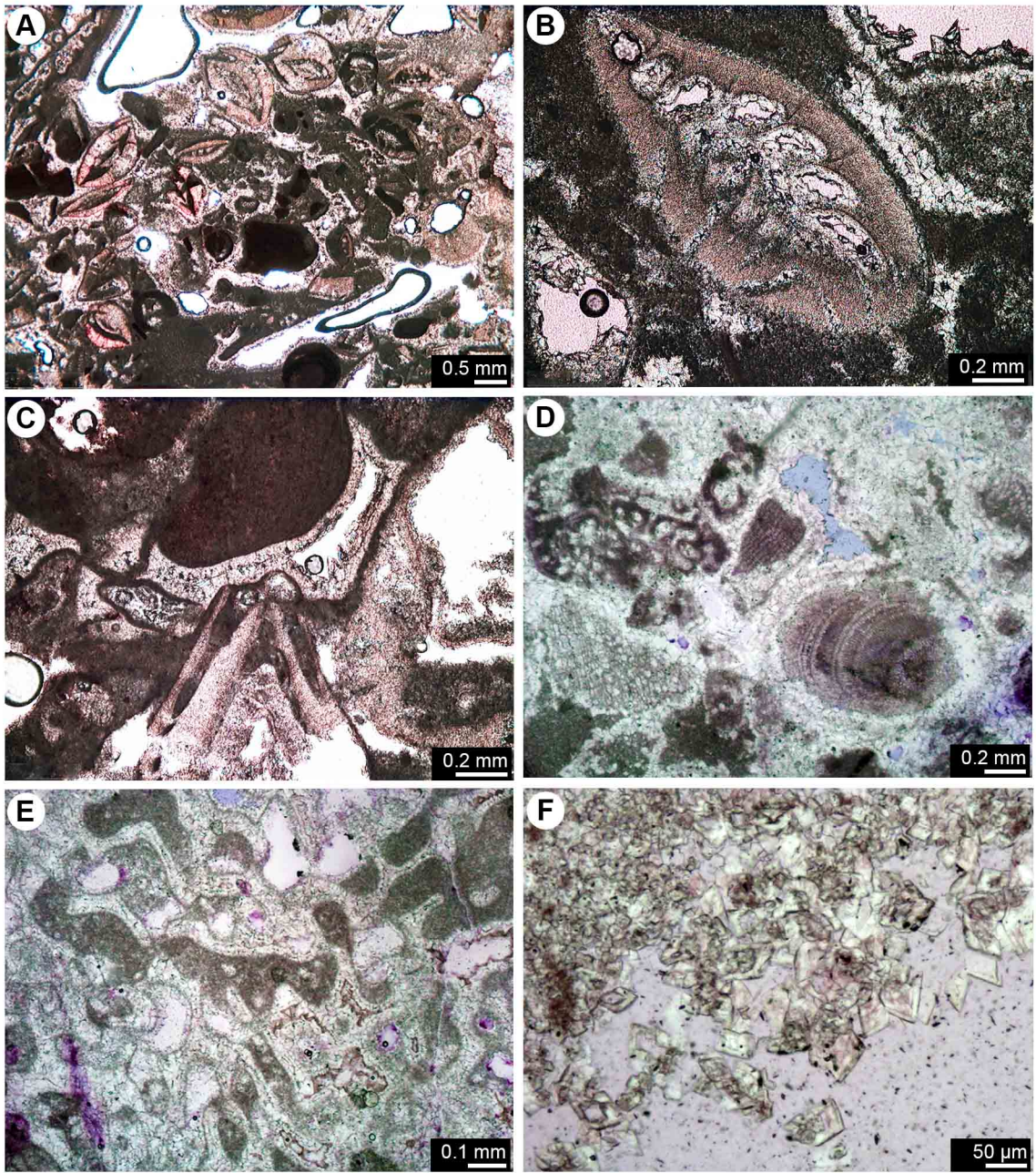


Fig. 8

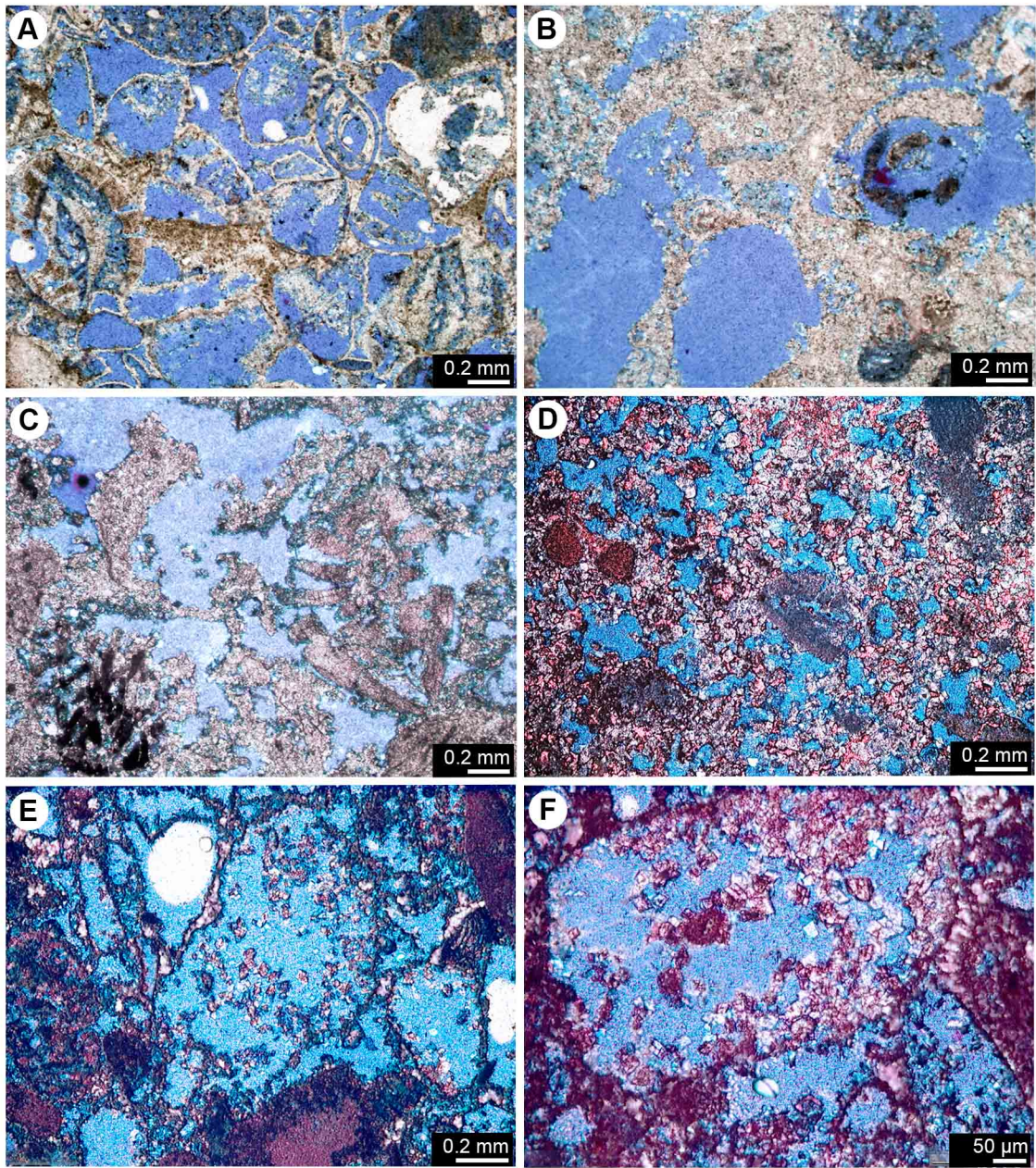


Fig. 9

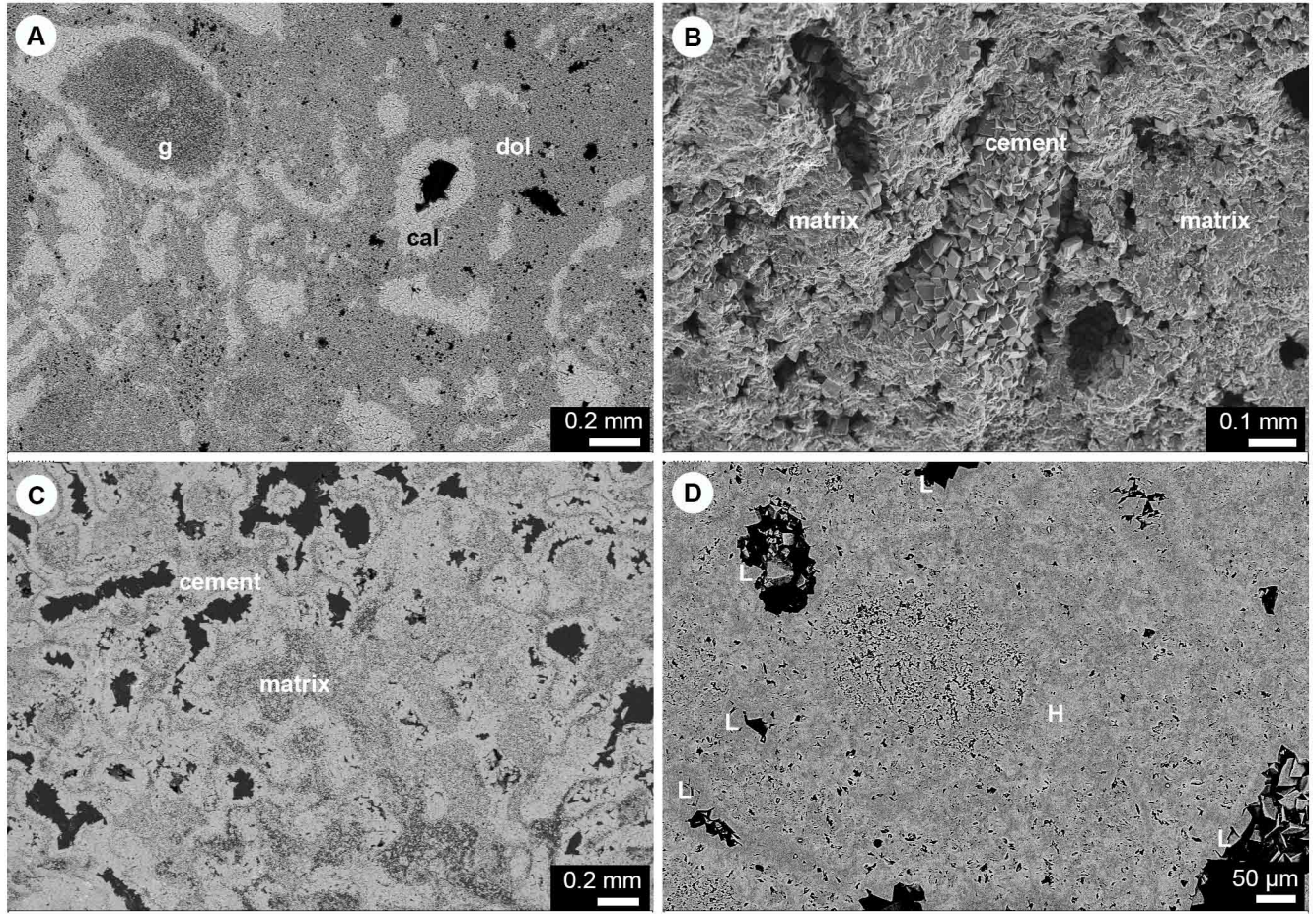


Fig. 10

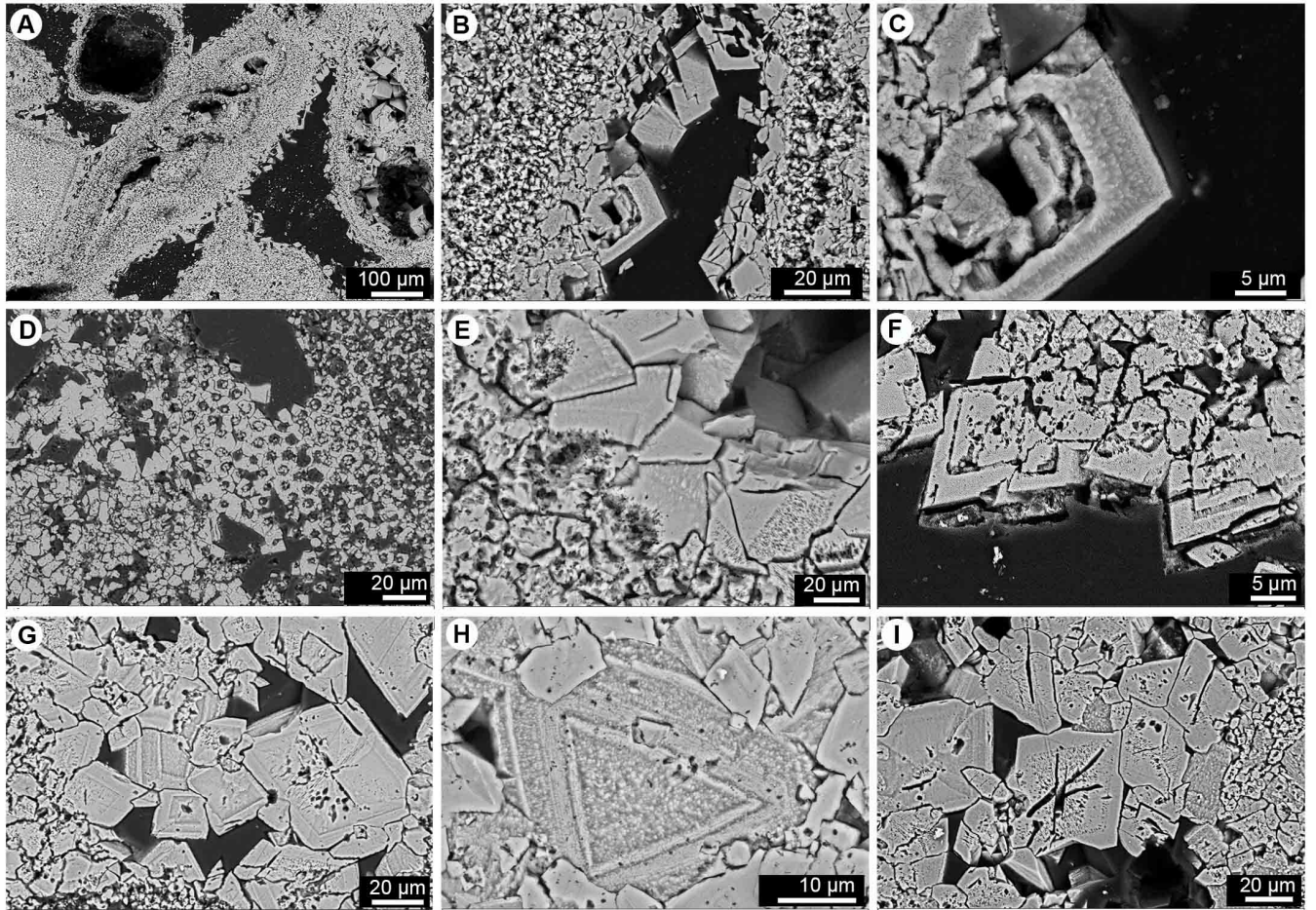


Fig. 11

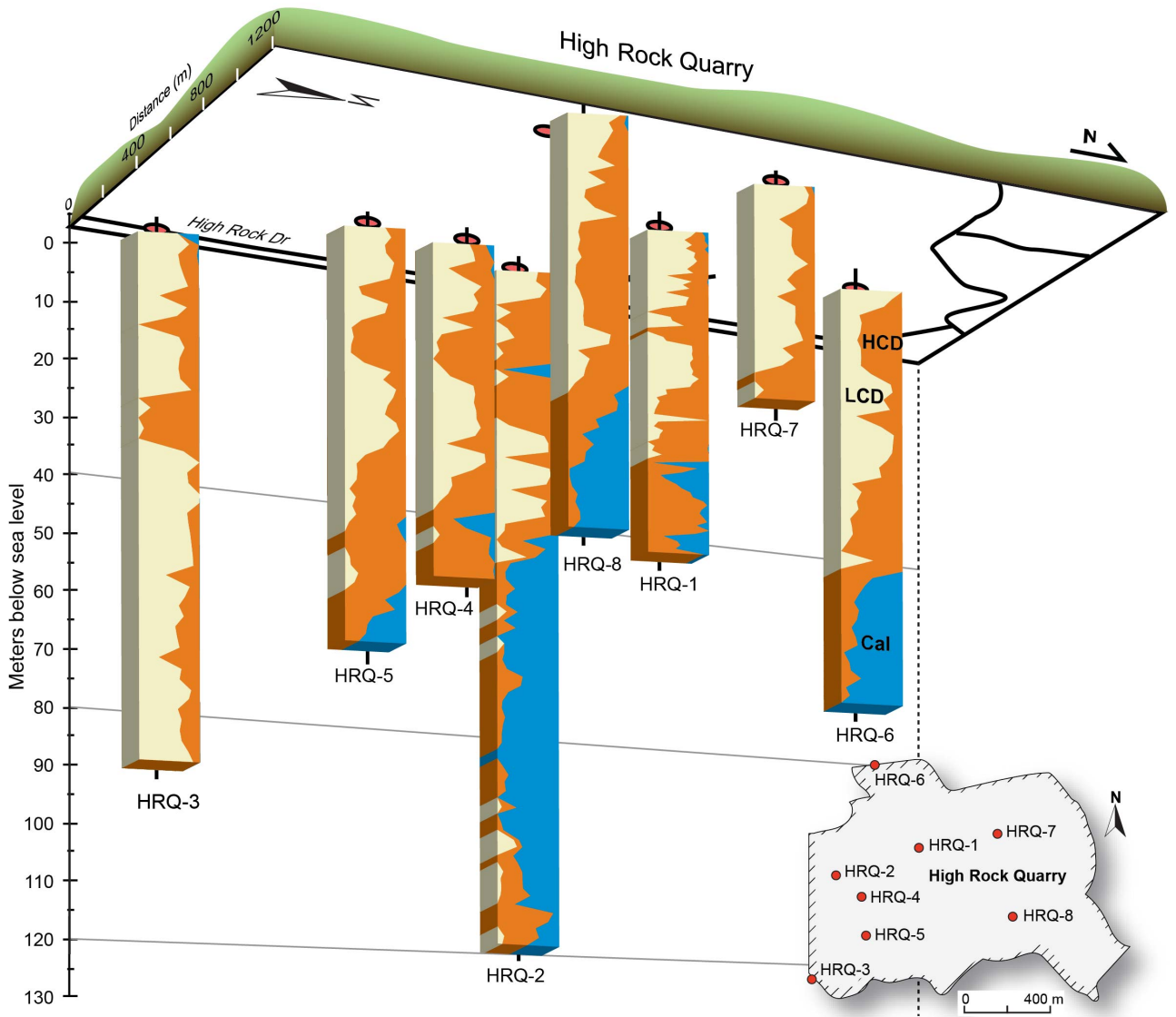


Fig. 12

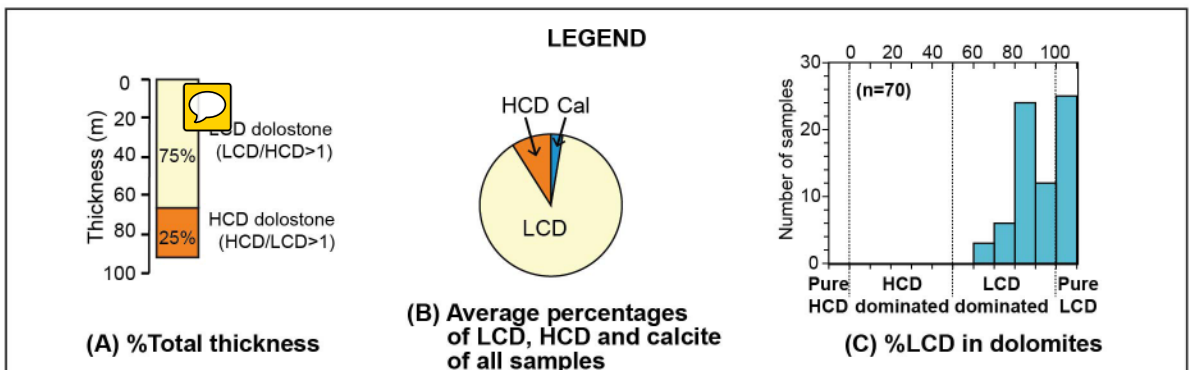
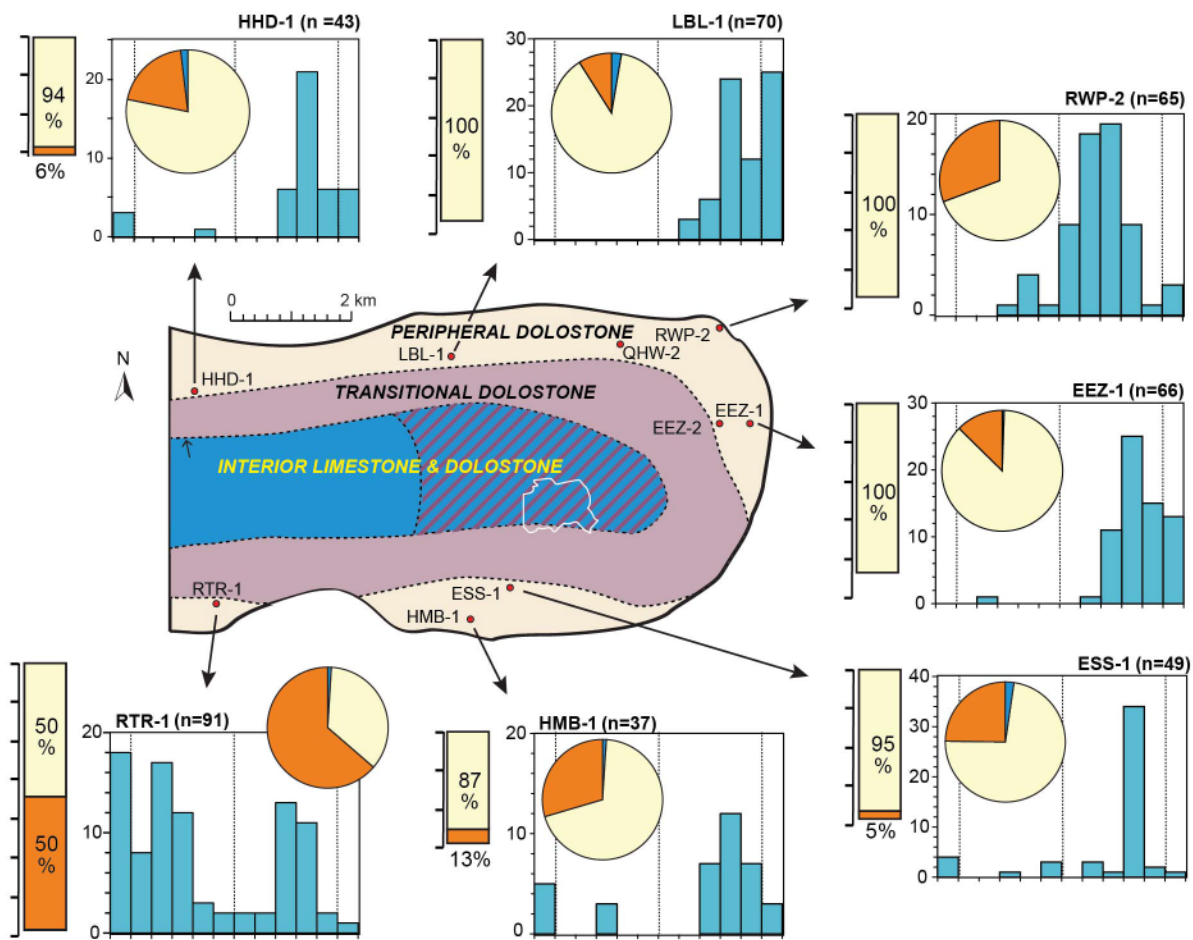


Fig. 13

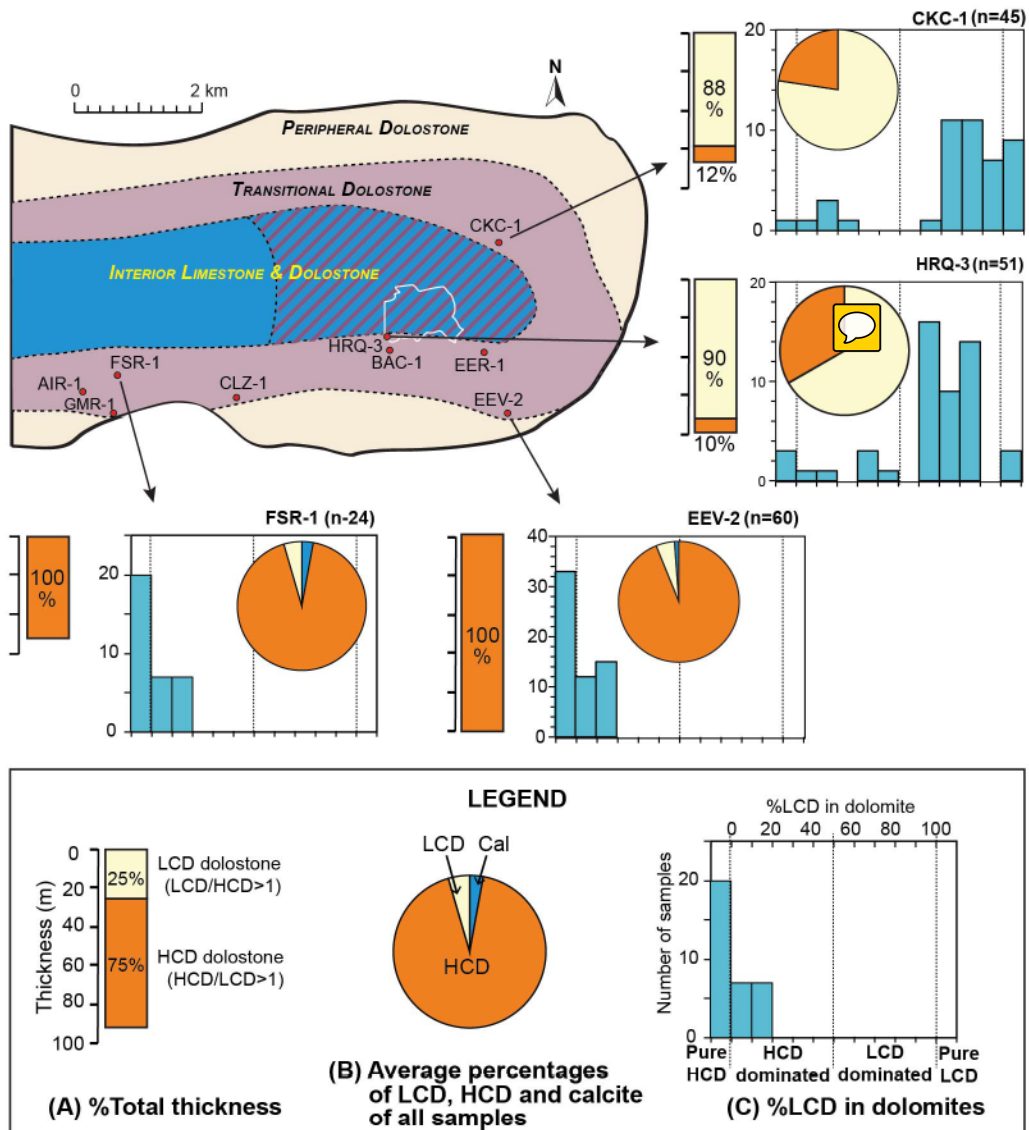


Fig. 14

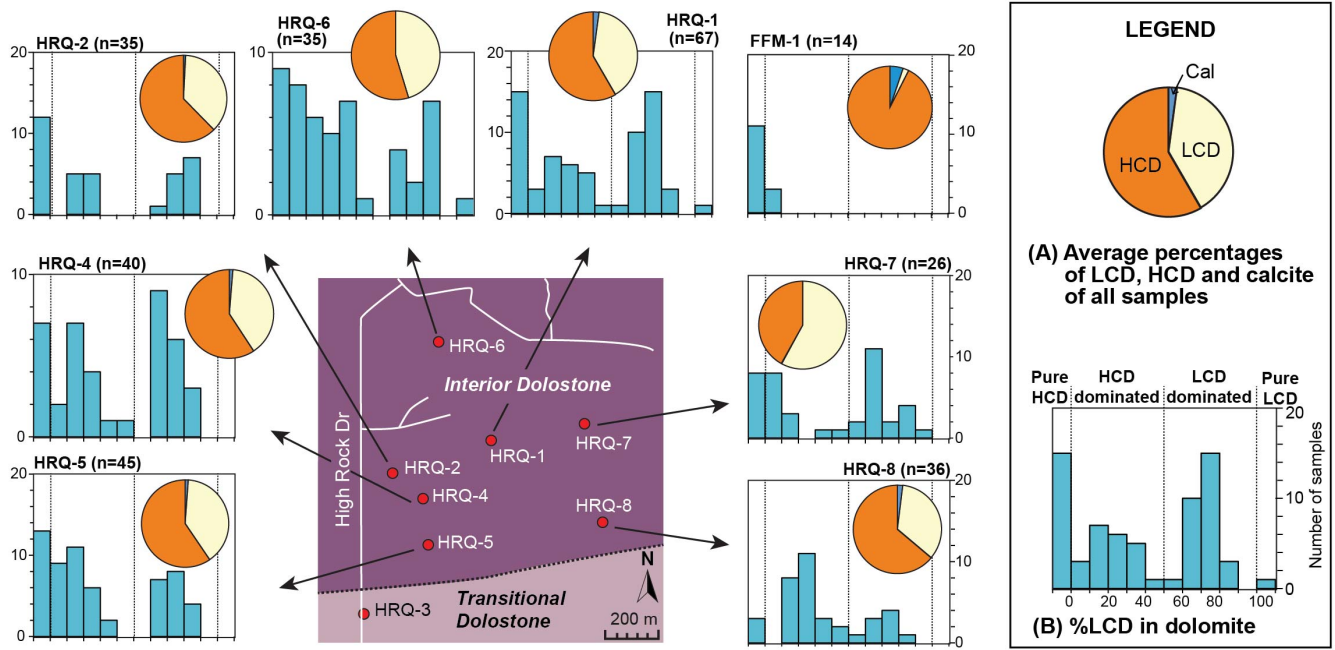


Fig. 15

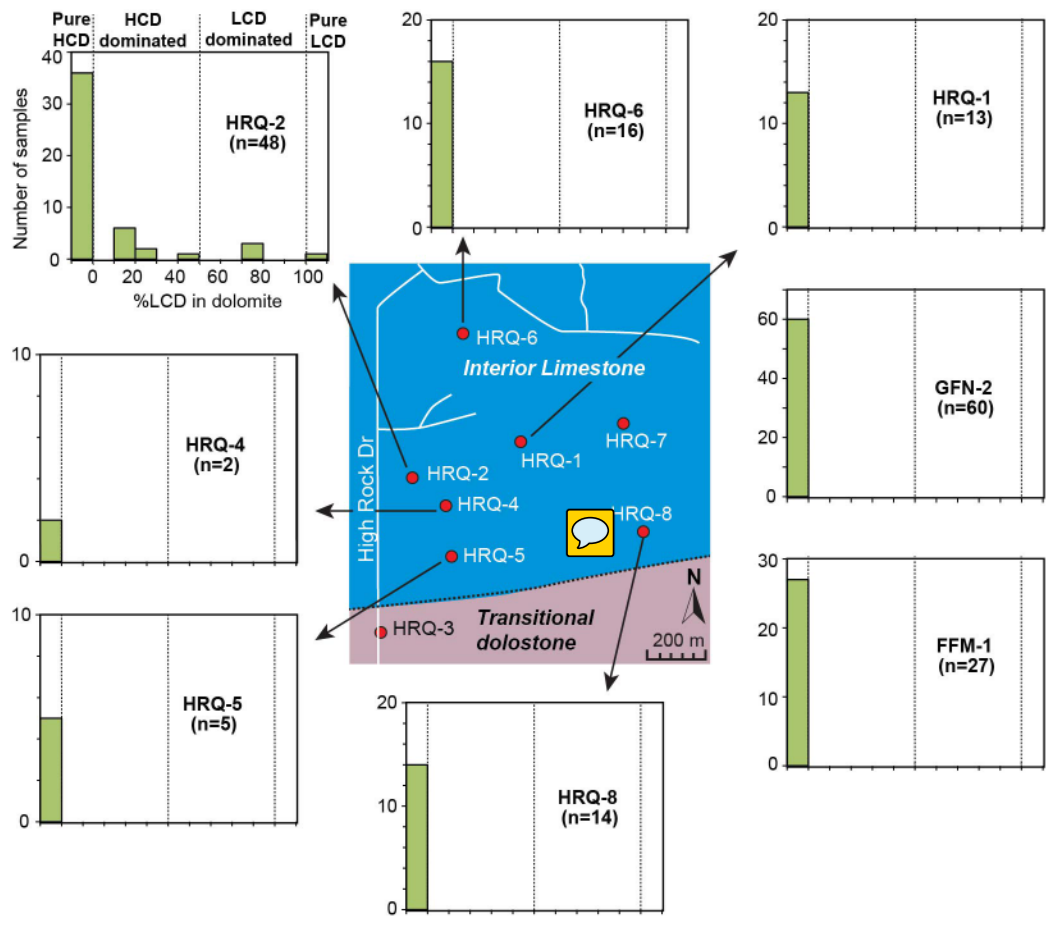


Fig. 16

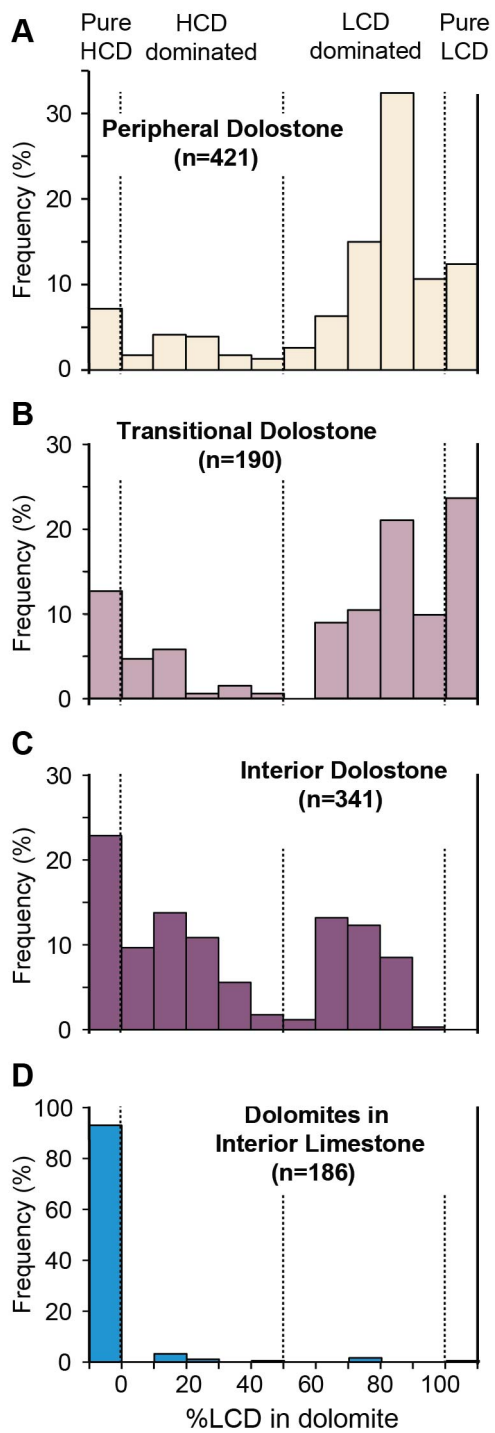


Fig. 17

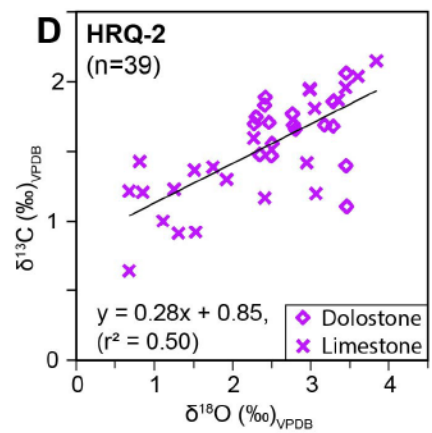
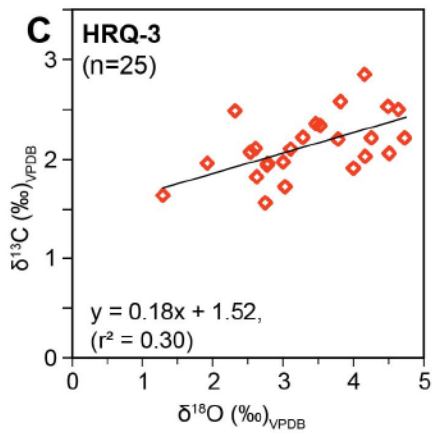
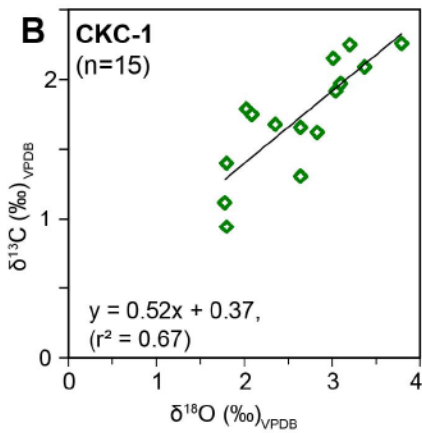
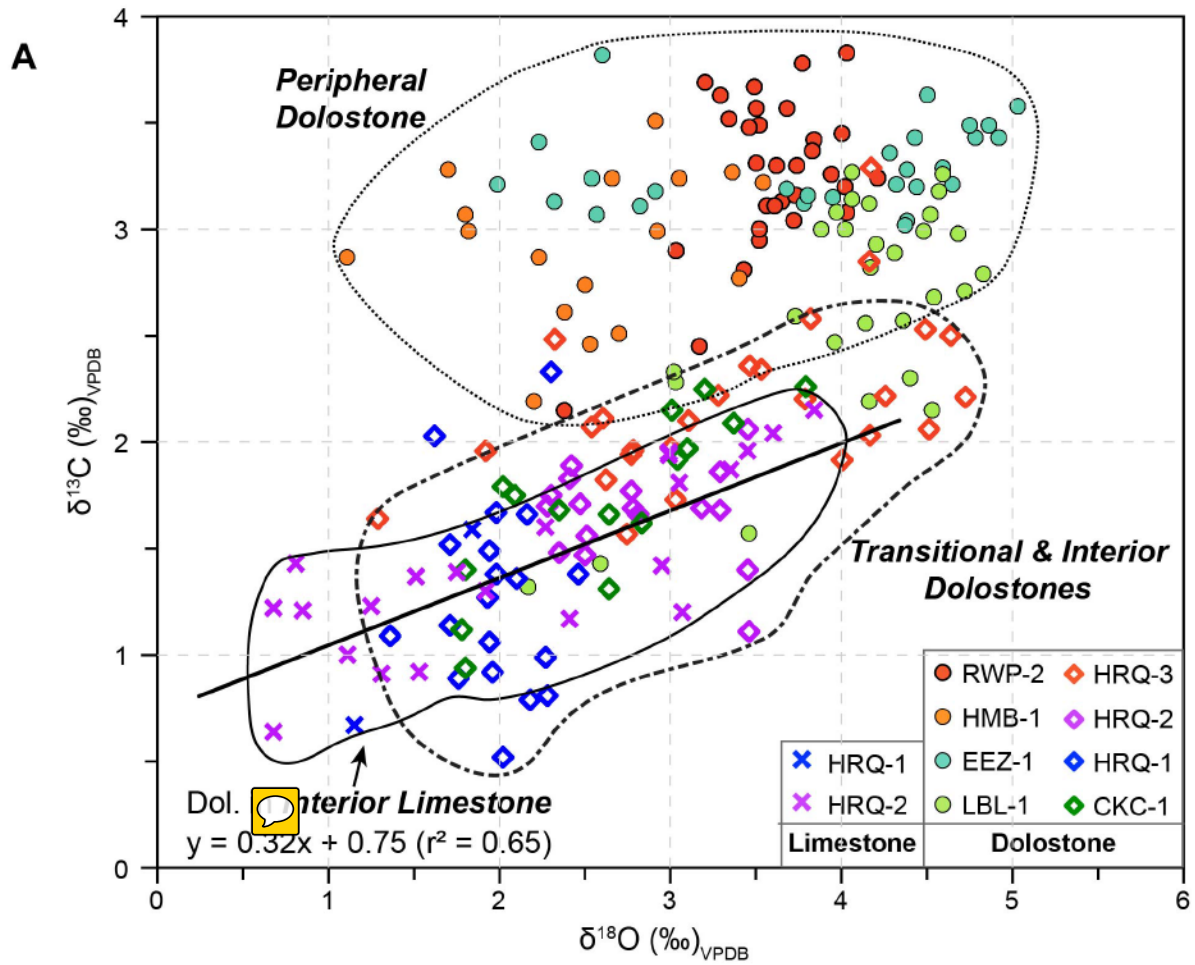


Fig. 18

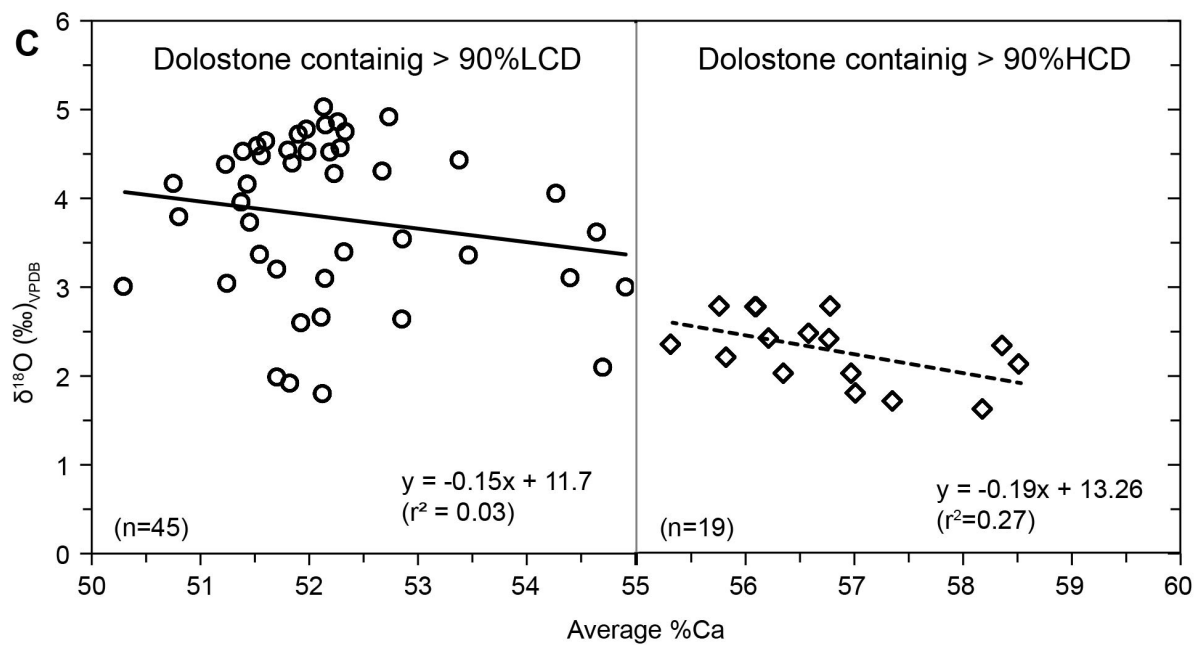
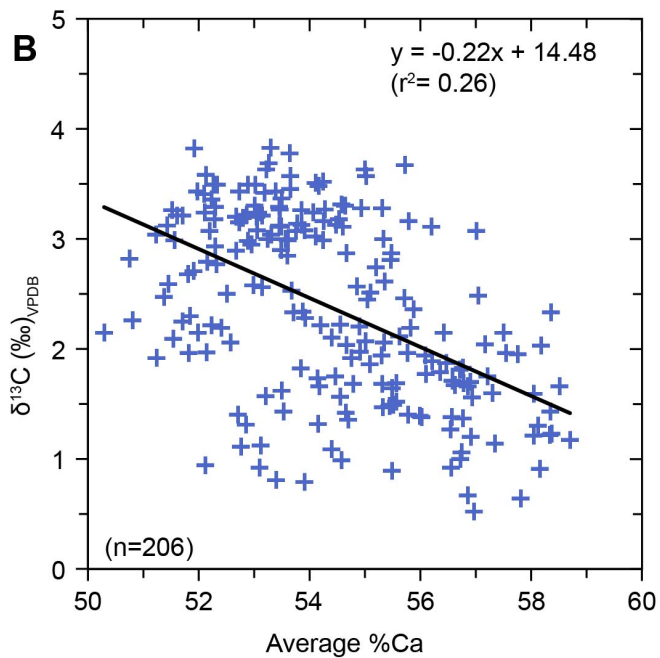
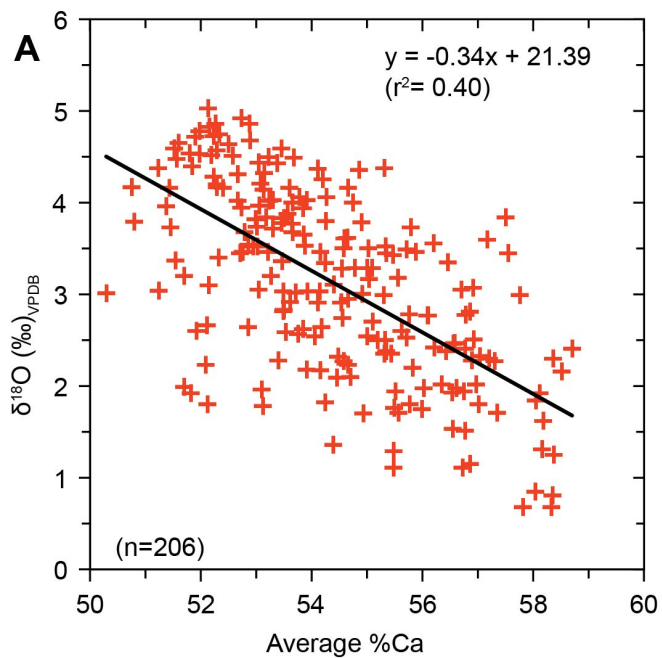


Fig. 19

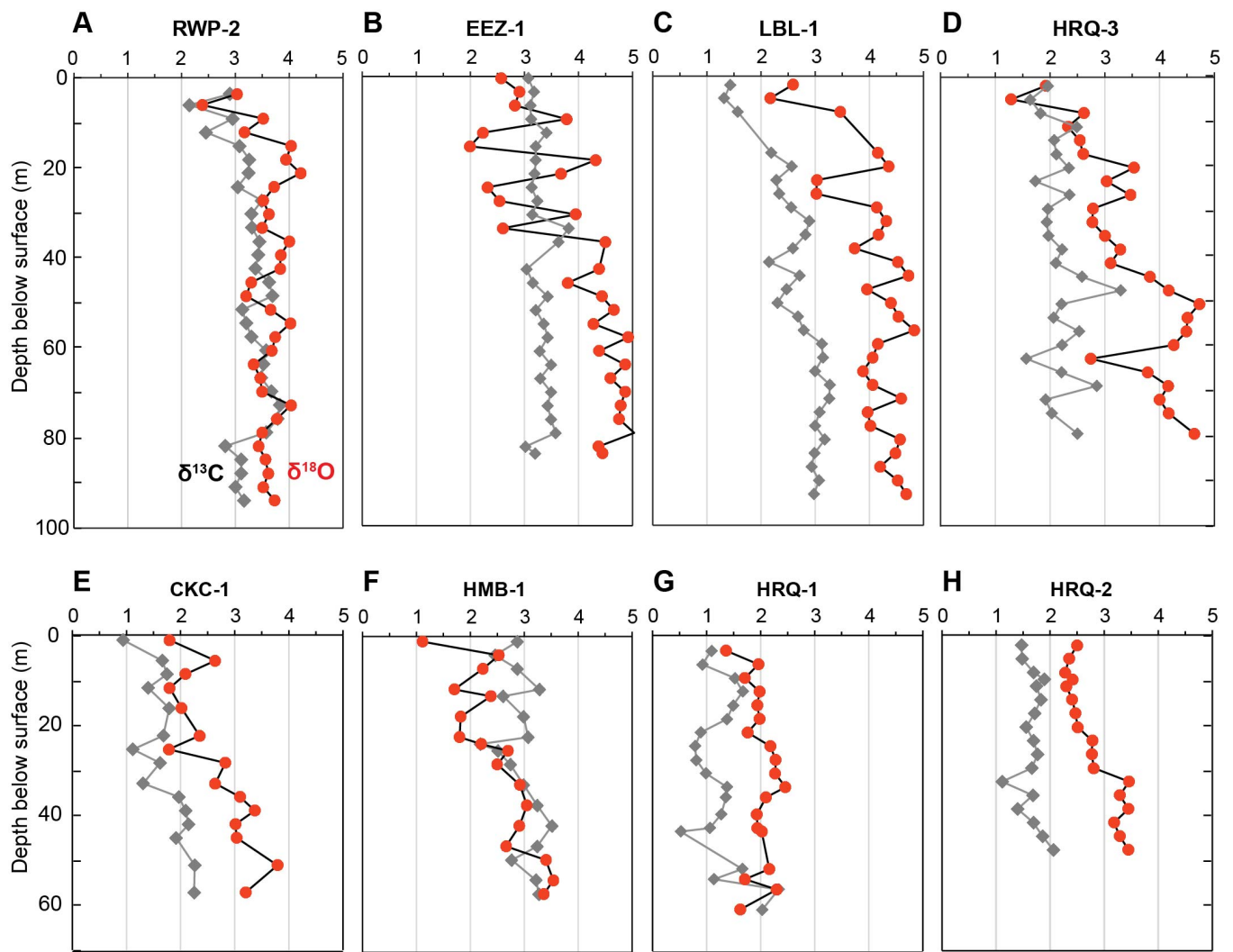


Fig. 20

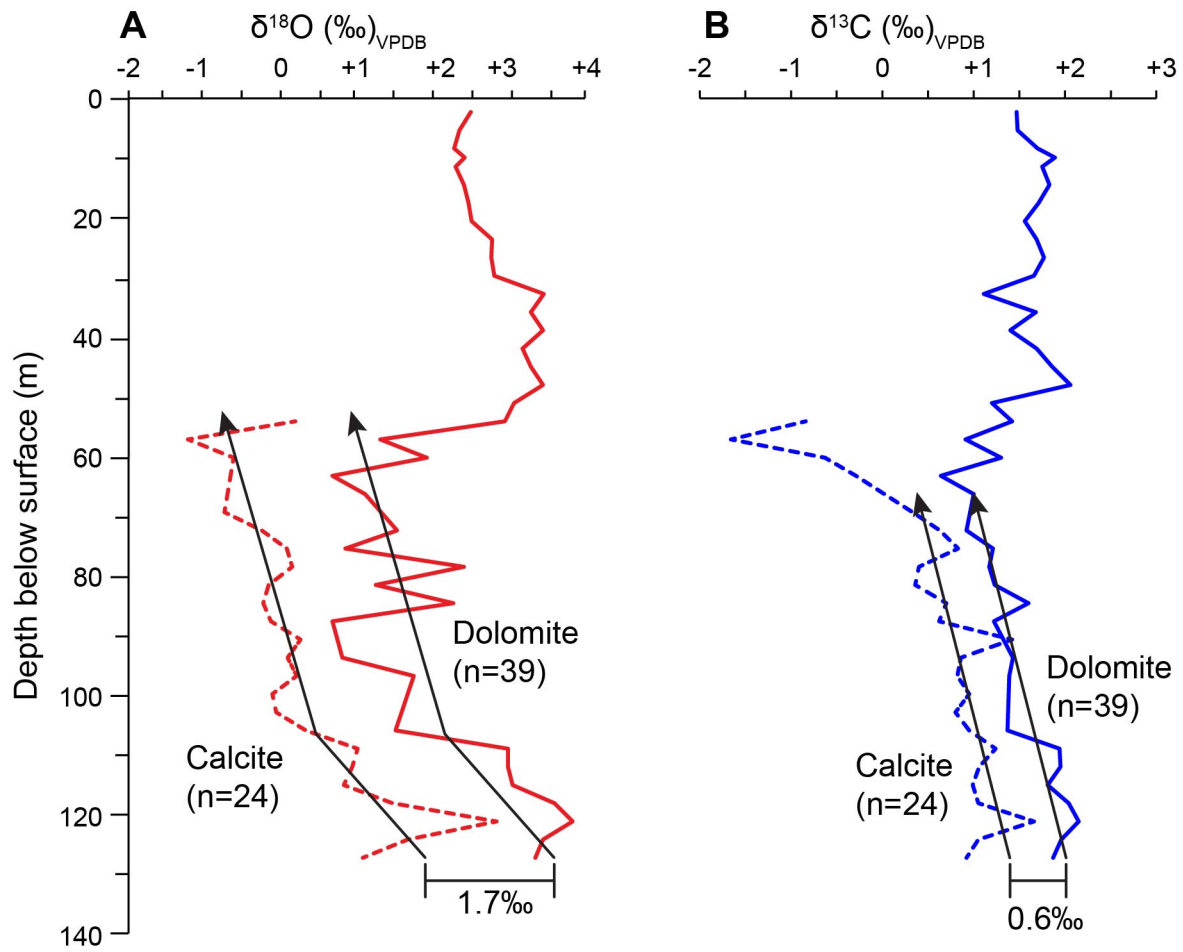


Fig. 21

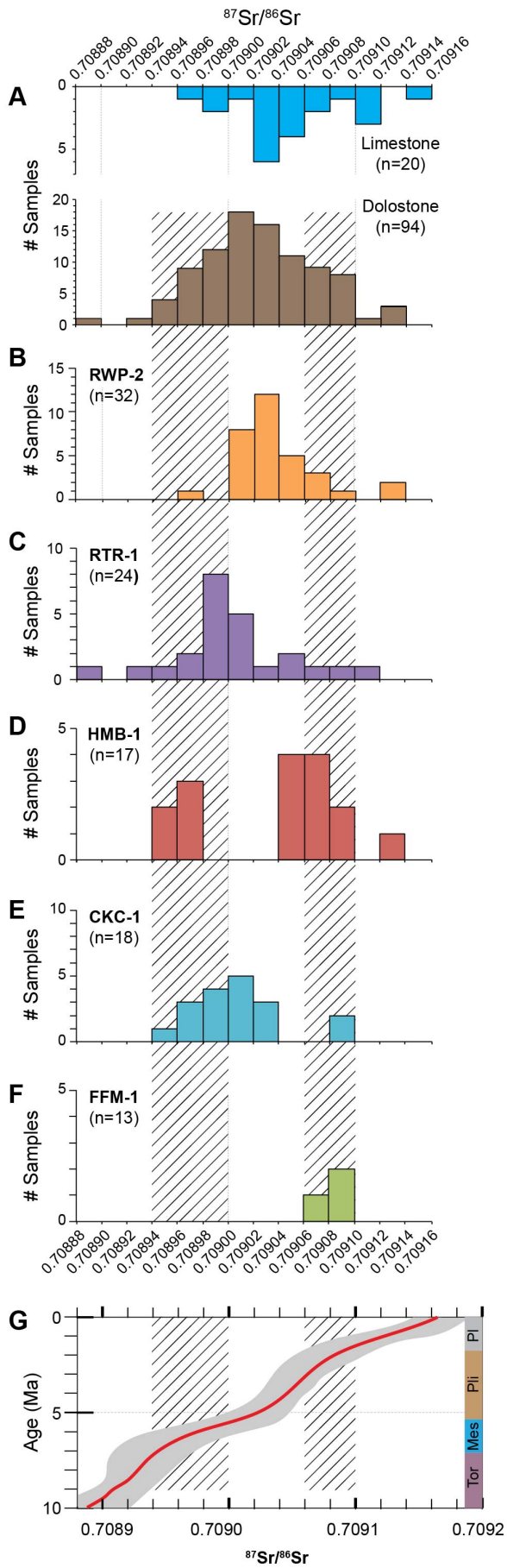


Fig. 22

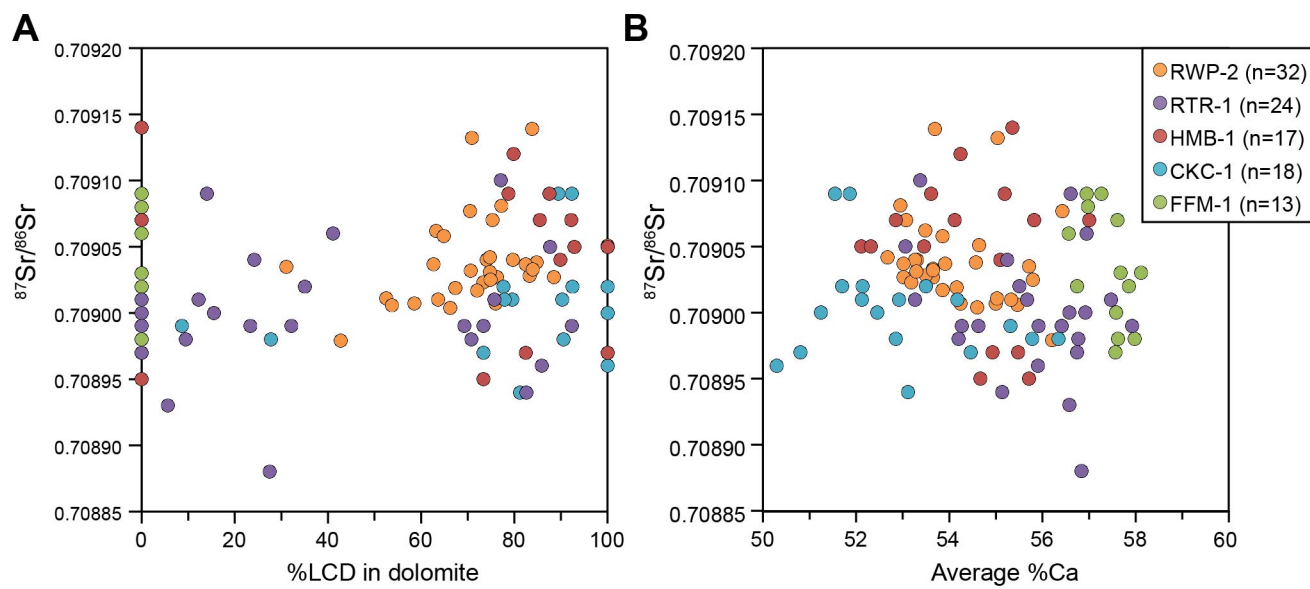


Fig. 23

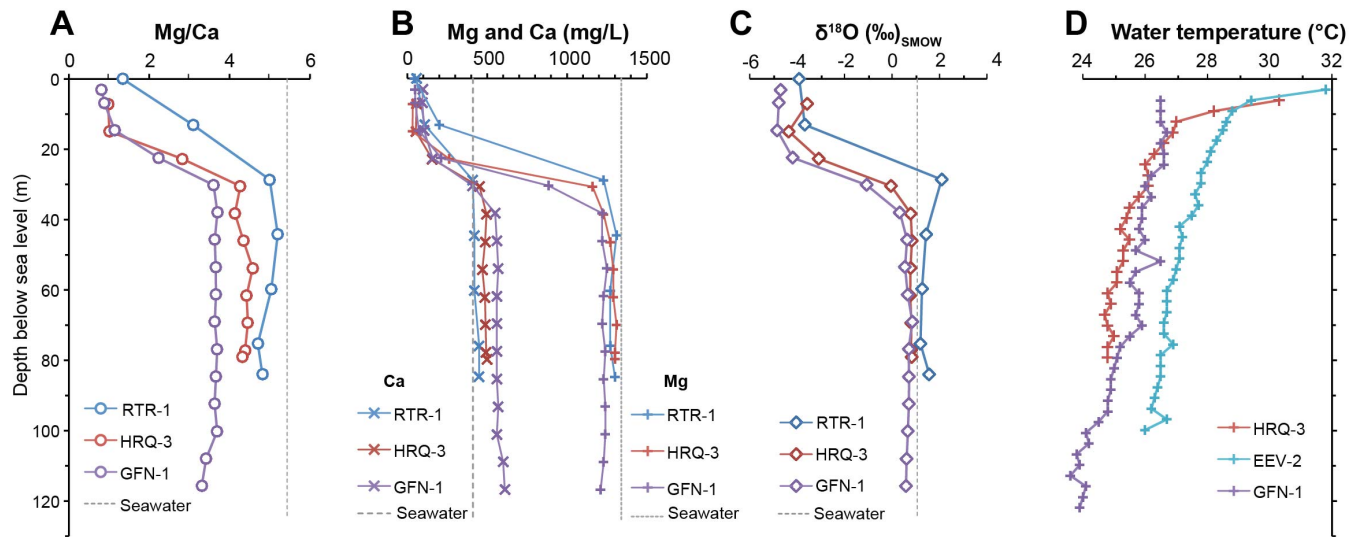


Fig. 24

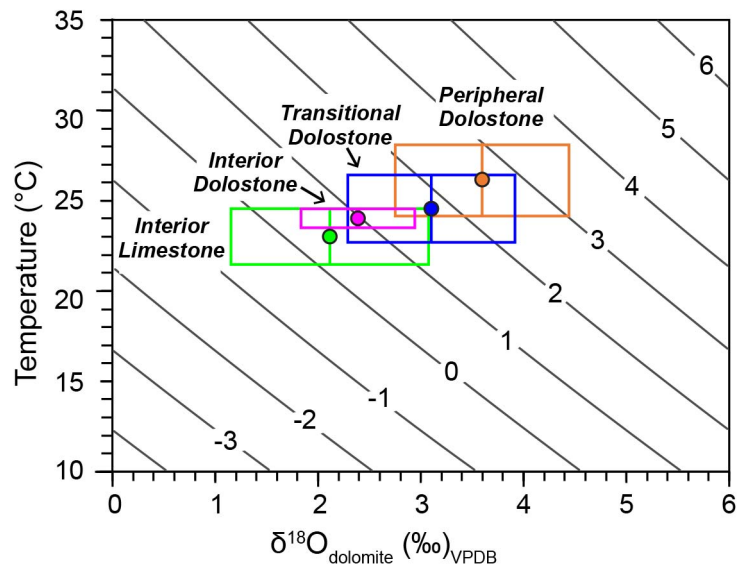


Fig. 25

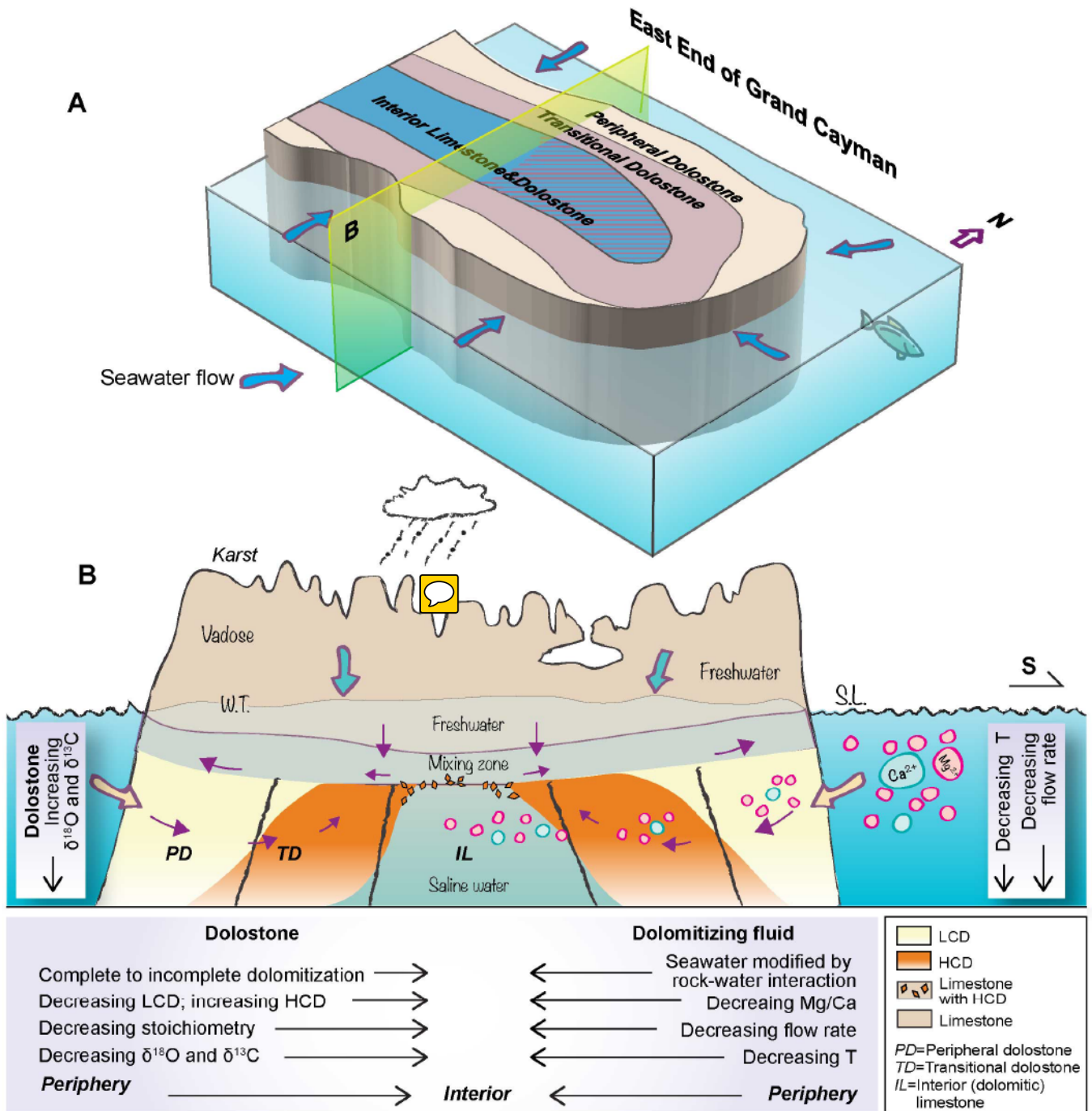


Fig. 26

1 **Tables**2 **Table 1**

3 Wells on the east end of Grand Cayman (see Figs. 1, 6 for locations) used this study.

4 Twenty-one wells (in bold) were the primary wells used in this study. Distance to shelf

5 edge is the shortest distances from the well to the northern (N), eastern (E), or southern (S)

6 shelf edge. (PD=peripheral dolostone, TD=transitional dolostone, IL/D=interior

7 limestone/dolostone, IL=interior limestone only).

Well	Zone	Total depth (m)	Distance to shelf edge (km)	%Core	%Cutting
<b>HHD-1</b>	PD	61.0	1.55 /N	0	100
<b>LBL-1</b>	PD	94.5	1.36 /N	0	chip
<b>RWP-2</b>	PD	94.6	0.66 /N	97	0
<b>EEZ-1</b>	PD	87.6	1.40 /E	0	chip
<b>ESS-1</b>	PD	77.4	1.29 /S	0	100
<b>HMB-1</b>	PD	57.9	0.86 /S	0	chip
<b>RTR-1</b>	PD	138.7	1.32 /S	0	100
QHW-1	PD	*60.0	1.16 /N		
EEZ-2	PD	87.6	1.86 /E		
<b>CKC-1</b>	TD	67.2	3.10 /E	0	chip
<b>EEV-2</b>	TD	101.8	1.14 /S	0	chip
<b>HRQ-3</b>	TD	80.0	2.48 /S	0	100
<b>FSR-1</b>	TD	**52.4	2.21 /S	0	chip
EER-1	TD	140.2	2.45 /S	0	chip
BAC-1	TD	39.6	2.22 /S	0	100
GMR-2	TD	46.0	1.45 /S	0	chip
AIR-1	TD	49.4	1.82 /S	0	chip
<b>GFN-2</b>	IL/D	92.2	2.75 /N	63	0
<b>FFM-1</b>	IL/D	64.8	3.42 /S	0	chip
<b>HRQ-2</b>	IL/D	128.0	3.00 /S	0	100
<b>HRQ-1</b>	IL/D	61.7	3.23 /S	0	100
<b>HRQ-4</b>	IL/D	64.0	2.95 /S	0	100
<b>HRQ-5</b>	IL/D	76.2	2.78 /S	0	100
<b>HRQ-6</b>	IL/D	76.2	3.55 /S	0	100
<b>HRQ-7</b>	IL/D	39.6	3.29 /S	0	100

<b>HRQ-8</b>	IL/D	76.2	2.90 /S	0	100
<b>DTE-1</b>	IL	**46.3	2.88 /S	0	chip
GFN-1	IL	122.3	2.75 /N	0	100
RAD-1	IL/D	20.1	3.43 /N	0	chip
EER-2	IL/D	115.8	2.73 /S	0	100
BOG-1	IL	39.6	2.75 /S	20	0
NSC-1	IL	***243.0	3.35 /S	0	chip

8 \* Cayman Formation in the lower 20 m (c.f., Jones and Luth, 2003b).

9 \*\*Cayman Formation starts ~8 m bsl.

10 \*\*\* Cayman formation in the upper ~140 m (c.f., Jones et al., 1994; Liang and Jones,

11 2014).